

## CHAPTER 9 SULFIDES

### 9.1 Introduction

Sulfides occur in many of the rocks in the Thompson Nickel Belt, but are most abundant in sulfide-facies iron-formations and associated metasedimentary rocks of the Pipe Formation, in ultramafic sills intruded into the Pipe Formation, and in associated ultramafic breccias (see **Chapter 5**). Because many sulfide phases, particularly chalcopyrite and pyrrhotite, are more ductile at high temperatures than many silicate phases, sulfide-rich rocks are more easily deformed than associated silicate-rich rocks (see reviews by Vokes, 2000; Marshall et al., 2000). Although the Fe-Ni-Cu-(PGE) sulfides in the TNB should have homogenized to monosulfide solid-solution (*MSS*) at such high metamorphic grades (upper amphibolite to granulite facies: **Chapter 3**) and recrystallized to low-temperature mineral assemblages during retrograde metamorphism, macroscopic and microscopic sulfide deformation structures, fabrics, and textures are well preserved in the TNB, recording a complex polyphase deformational history (see Bleeker, 1990b and **Chapter 6**).

Although the sulfides in the TNB are more deformed than those in most other magmatic Ni-Cu-(PGE) deposits, their mineralogy is similar to other deposits of this type (Leshner, 1989; Leshner & Keays, 2002). Primary (i.e., non-supergene) ores are dominated by pyrrhotite-pentlandite, pyrrhotite-pentlandite-pyrite, and less common pentlandite-pyrite and pentlandite-pyrite-millerite assemblages (Bleeker, 1990b; Liwanag, 2001). Chalcopyrite, magnetite, and ferrochromite are ubiquitous minor phases. Magnetite is more abundant in disseminated and net-textured ores, whereas pyrite is more abundant in massive ores.

The purpose of this chapter is to describe and interpret the textures, mineralogy, mineral chemistry, and whole-rock chemistry of the sulfide-bearing rocks in the TNB. The textural descriptions, mineralogy, and mineral chemistry are largely from Liwanag (2001) and are based on samples taken from the Thompson mine (T1, 1C, 1D), which occurs in member Op1 of the Pipe Formation, the Birchtree mine, which occurs in member Op2 of the Pipe Formation, and the William Lake ultramafic bodies, which occur in an undetermined part of the Pipe Formation.

### 9.2 Mineralization Status

Rocks in magmatic Ni-Cu-Co-(PGE) sulfide deposits are generally classified as **ore** or **waste** on the basis of the *Ni equivalent* cut-off grade ( $Ni_{EQ}$ ), which is the grade at which the rock is profitable to mine expressed in terms of the Ni content adjusted for the abundances of less valuable Cu and more valuable Co and PGEs.

However, from a genetic standpoint it is more desirable to classify rocks and ores as **economically mineralized** (above cut-off grade), **uneconomically mineralized** (below cut-off grade, but containing genetically-significant amounts of Ni-Cu-Co-PGE mineralization), or **non-mineralized** (barren of magmatic Ni-Cu-Co-PGE mineralization). However, it is difficult to apply classifications of this type in an area where many different ore types are present (e.g., ultramafic-hosted, ultramafic breccia-hosted, metapelite-hosted, and iron formation-hosted) because each rock has a different non-sulfide Ni content. For example, the analytical data presented in **Chapter 8** indicate that olivines (excluding those interpreted to be enriched or depleted in Ni) contain up to 3500 ppm Ni and that barren meso- to adcumulate ultramafic rocks contain up to ~3000 ppm Ni. On this basis, *ultramafic cumulate*

rocks containing  $\leq 3000$  ppm should be referred to as “barren” and those containing  $> 3000$  ppm Ni should be referred to as “mineralized”. Similarly, the analytical data in **Chapter 8** indicate that pelitic schists and silicate-facies iron-formations in the Pipe Formation normally contain  $< 75$  ppm Ni, whereas sulfide-facies iron-formations contain up to 250 ppm Ni. On this basis, *metapelites* (and silicate-facies iron-formations) containing  $\leq 75$  ppm and *sulfide-facies iron-formations* containing  $\leq 250$  ppm should be referred to as “barren”, and those containing  $> 75$  ppm and  $> 250$  ppm, respectively, should be referred to as “mineralized.” Other rock types (e.g., metapyroxenites, metapicrites, metabasalts) will have intermediate cut-offs. It is possible to derive expressions that relate background (non-sulfide) Ni contents to the Mg contents of igneous rocks based on geochemical models, but such methods are not applicable to sedimentary rocks, especially those containing a mixture of detrital and volcanic-exhalative components.

Another way to approach this problem is to consider the metal content of the sulfide fraction of the rock, assuming that “barren” rocks contain only Fe sulfides (pyrrhotite, pyrite) but that “mineralized” rocks also contain Fe-Ni-Cu sulfides (pentlandite, chalcopyrite). However, recalculating metal abundances to 100% sulfides requires knowledge of the compositions of the sulfides, which vary from sample to sample (see below), and involves many assumptions and magnifications of errors, especially for rocks containing only small amounts of metals that may be housed in a variety of sulfide, silicate, oxide, and alloy phases. For example, an unaltered dunite that contains cotectic proportions of olivine ( $\sim 98.4\%$ ) with  $\sim 3500$  ppm Ni and fine disseminated sulfides ( $\sim 1.6\%$ ) with  $\sim 15\%$  Ni contains  $\sim 3440$  ppm silicate Ni and  $\sim 2460$  ppm sulfide Ni, whereas the same rock if completely serpentinized (in which all of the Ni has been mobilized into sulfides) contains  $\sim 5900$  ppm sulfide Ni. Similarly, the Ni contents of pyrrhotites may vary considerably, exceeding 1% in some non-mineralized sedimentary rocks (see below). Because the error magnifications and relative contributions of silicate Ni are less significant in samples that contain greater amounts of sulfides, calculations of this type should be restricted to mineralized samples, making this method less valuable for establishing the mineralization status of sulfide-poor samples.

Most magmatic sulfide ores also contain significant amounts of magnetite and ferrochromite, which are commonly ignored in calculations of this type. All of the ferrochromite and much of the magnetite undoubtedly crystallized from the sulfide magma and reflect significant amounts of dissolved O (Doyle and Naldrett, 1987), but these phases contain only small amounts of ore metals, except in the absence of any sulfides.

Accepting these limitations, we have recalculated the compositions of semi-massive and massive sulfide samples to 100% sulfides assuming that all of the Cu is in stoichiometric chalcopyrite with a composition of  $\text{CuFeS}_2$  ( $\sim 34.6\%$  Cu,  $\sim 34.9\%$  S), that all of the Ni is a typical TNB pentlandite with an average composition of  $\text{Fe}_{4.3}\text{Ni}_{4.7}\text{S}_8$  ( $33.2\%$  Fe,  $36.0\%$  Ni,  $33.2\%$  S), and that the remainder of the S is in monoclinic pyrrhotite with a composition of  $\text{Fe}_{0.875}\text{S}$  ( $\sim 60.4\%$  Fe,  $\sim 39.6\%$  S). The raw abundances of metals in whole rocks are indicated in terms of their usual elemental symbols (Ni, Cu, Co, PGE), whereas those that have been recalculated to 100% sulfides are indicated with a subscript ( $\text{Ni}_{100}$ ,  $\text{Cu}_{100}$ ,  $\text{Co}_{100}$ ,  $\text{PGE}_{100}$ ).

### 9.3 Ore Types

Komatiite-associated nickel sulfide deposits are part of a continuum of lithotectonic associations in the family of magmatic Ni-Cu-PGE deposits, which contains a variety of

mineralization types (Leshner and Keays, 2002): **Type I** stratiform basal massive\net-textured\disseminated mineralization, **Type II** strata-bound internal disseminated mineralization, **Type III** stratiform “reef-style” mineralization, **Type IVa** Ni-enriched metasediment mineralization, **Type IVb** hydrothermal mineralization, and **Type V** tectonic “offset” mineralization. Types I-II-(III) ores are analogous to the “intraparenatal” ores of Bleeker (1990), whereas Type V ores are analogous to the “extraparenatal” ores of Bleeker (1990), respectively.

## 9.4 Sulfide Textures

### 9.4.1 Textural Classification

Although the sulfides in the TNB are much more deformed than those in many other deposits of this type, the distributions and textures of the ores are broadly similar (**Table 9.1**).

**Table 9.1** Sulfide ore types, textures, distributions, and host rocks in the TNB (adapted and expanded from Bleeker, 1990b and Liwanag, 2001)

Sulfide Abundance	Sulfide Texture	Rock Texture	Sulfide Distribution	Host Rock		
				Meta-Sediment	Ultramafic Rock	Ultramafic Breccia
≤10%	Disseminated	diverse	interstitial	DS-SED <b>DS-SED</b>	<b>DS-U</b>	<b>DS-UB</b>
10-40%	Heavy Disseminated Patchy Disseminated Blebbly Disseminated	diverse	interstitial to intercumulus	HDS-SED <b>HDS-SED</b>	<b>HDS-U</b> <b>PDS-U</b> <b>BS-U</b>	<b>HDS-UB</b> <b>PDS-UB</b>
	Layered	laminated to banded	interstitial to intergranular	LS-SED <b>LS-SED</b>	—	—
40-70%	Net-Textured	meso- to adcumulate	intercumulus	—	<b>NS-U</b>	—
	Semi-Massive	schistose, gneissic, mylonitic	intergranular	SMS-SED <b>SMS-SED</b>	—	<b>SMS-UB</b>
>70%	Massive	cataclastic, blastomylonitic	—	MS-SED <b>MS-SED</b>	—	<b>MS-UB</b>

**Notes:** All textures and abundances are gradational. Abbreviations based on textural type, host rock, and mineralization status; **S** = barren Fe sulfides, **S** = Fe-Ni-Cu sulfides.

### 9.4.2 Textural Descriptions

**DS-SED:** Barren disseminated sulfides (**Fig. 9.1a**) in metasediments are composed primarily of fine- to medium-grained, foliated pyrrhotite patches or euhedral trains of pyrite, or both. Sulfides adjacent to or near ultramafic rocks may also contain very fine-grained angular to rounded patches of pentlandite and/or chalcopyrite (**Figs. 9.1b** and **9.1c**).

**SMS-SED** and **MS-SED:** Barren semi-massive and massive sulfides in metasediments occur as mm- to dm-scale layers of pyrrhotite (**Fig. 9.3a**). Pyrrhotite is typically fine-grained and annealed, and comprises both hexagonal and monoclinic polymorphs. The sulfides do not contain macroscopic pentlandite and are normally graphitic, commonly containing up to 25% graphite. Graphite occurs as foliated single inclusions in sulfides or as aggregates associated

with foliated biotite flakes and rounded to subrounded quartz and plagioclase (**Fig. 9.3b**). Chalcopyrite, pyrite, and magnetite are present in minor to trace amounts. Chalcopyrite typically occurs as very fine-grained blebs within pyrrhotite and as “porous” masses adjacent to silicate inclusions. Pyrite occurs as subhedral aggregates replacing pyrrhotite. Magnetite occurs as randomly distributed, fine-grained, anhedral grains. Up to 5% pentlandite occurs microscopically as “flames” and very fine-grained “chains” at the boundaries of annealed pyrrhotite grains in a few samples (e.g., JL99-1D-37, JL99-1D-38, JL99-1D-39: **Fig. 9.3b**).

**SMS-SED and MS-SED:** Mineralized semi-massive to massive sulfides in metasediments occur at the contacts between ultramafic bodies and barren metasediments (interpreted to be largely in place) and isolated within barren metasediments (interpreted to have been mobilized from ultramafic contacts). They are composed of mainly pyrrhotite and pentlandite (**Fig. 9.5a**) with minor amounts of chalcopyrite, pyrite, magnetite, ferrochromite, and gersdorffite [NiAsS]. Pyrrhotite occurs as annealed polygonal grains. Pentlandite occurs as i) very fine lamellae, ii) elongated, wispy “chains” (**Fig. 9.5b**), and iii) coarse-grained, subangular to subrounded “eyes” (**Fig. 9.5c**) that are typically <1mm to 5 mm, but range up to 2 cm in some horizons. In many massive sulfide horizons in the Thompson Mine, pentlandite eyes are often segregated into cm-scale bands within a coarse-grained, annealed pyrrhotite matrix (**Fig. 9.12b**). Pyrite typically occurs as aggregates of subhedral grains that replace both pentlandite and pyrrhotite (**Fig. 9.6**). Gersdorffite occurs as very fine, anhedral to subhedral grains (**Fig. 9.6**). Magnetite and chromite occur as very fine-grained euhedral to subhedral grains randomly oriented in a sulfide matrix. The margins of massive sulfide horizons commonly show evidence of brecciation along the contacts with hosting metasedimentary rocks (**Fig. 9.7**). Fine- to coarse-grained chalcopyrite typically occurs adjacent to pentlandite in stringers that project into the metasedimentary rocks along the contact (**Fig. 9.8**). Chalcopyrite is also concentrated adjacent to silicate inclusions (**Fig. 9.9**). Pyrite-chalcopyrite symplectites are irregularly distributed within and along the margins of the massive sulfide horizons (**Fig. 9.10**).

**DS-U, HD\$, and NS-U:** Mineralized disseminated and net-textured sulfides in ultramafic rocks range from fine-grained interstitial disseminations through lobate intercumulus grains to coarse-grained interstitial networks (**Fig. 9.2a**). Disseminated sulfides typically occur in the interior parts of ultramafic bodies, whereas net-textured sulfides typically occur in the exterior parts of the bodies. The sulfides comprise mainly pyrrhotite and pentlandite with minor chalcopyrite and magnetite. Pentlandite and chalcopyrite typically form subangular to subrounded patches along the edges of pyrrhotite grains (**Fig. 9.2b**). Magnetite typically occurs as fine anhedral grains adjacent to sulfides and as lamellae in silicates (**Fig. 9.2c**).

**SMS-UB and MS-UB:** Mineralized semi-massive and massive sulfides in ultramafic breccias form the matrix component of the breccias (**Fig. 9.4a**). Breccia fragments are fine- to very coarse-grained, tectonized inclusions of the host ultramafic rocks. The textures of the sulfides are similar on a microscopic scale to those in metasedimentary rocks (see above). The sulfide mineralogy is dominated by pyrrhotite and pentlandite, with minor amounts of chalcopyrite, pyrite, chromite, and gersdorffite. Pyrrhotite occurs as annealed medium- to coarse-grained polygonal grains. Pentlandite occurs as i) very fine lamellae (**Fig. 9.4b**), ii) elongated, wispy “chains”, and iii) coarse-grained, subangular to subrounded “eyes” (**Figs. 9.4b and 9.4c**). Pentlandite eyes are typically <1mm to 5 mm. Gersdorffite occurs as very fine, anhedral to subhedral grains (**Figs. 9.5b and 9.5c**).

Isothermal and controlled cooling experiments on monosulfide solid-solution (*MSS*) by Durazzo and Taylor (1982), as well as previous work by Naldrett et al. (1967), Ewers (1972), Misra and Fleet (1974), and McQueen (1979), suggest that the pentlandite grains occurring as equant blebs or as chain-like aggregates along the boundaries between annealed pyrrhotite grains (location E<sub>2</sub> in **Fig. 9.15**) formed from *MSS* that cooled from temperatures between 610° and 250°C. At temperatures below 250°C, lower diffusion rates of Fe and Ni may prevent continuous re-equilibration and produce higher degrees of supersaturation than is possible at higher temperatures (Durazzo and Taylor, 1982). Coarsened linear pentlandite, including wedges and elongated aggregates developed along one direction within the *MSS* matrix, probably exsolved from *MSS* between 250°-150°C. Thin, fine-grained, linear pentlandite, commonly referred to as pentlandite “flames” (e.g. **Fig. 9.4b**), probably exsolves at 150°C or slightly below. Thus, the common occurrence of a combination of pentlandite textures within individual sulfide samples throughout the TNB indicates complex cooling history involving several generations of equilibration.

#### 9.4.3 Textural Variations Between Ore Deposits

The mineralized semi-massive to massive sulfide samples collected from various deposits in the Thompson Nickel Belt for this study (8 from Birchtree, 10 from T1, 10 from 1C, 15 from 1D, and 12 from William Lake) can be characterized in terms of host rock, proximity to ultramafic boudins, inclusion population (which can comprise up to 60% of the sample), and macroscopic texture of pentlandite.

**Birchtree:** The ores in the Birchtree mine are M\$-UB that occur in ultramafic boudin necks and at the bases of ultramafic bodies. They contain randomly-oriented to oriented, medium- to coarse-grained brecciated ultramafic inclusions and minor pelitic inclusions. Pyrrhotite, the principal sulfide phase, is associated with up to 10% fine- to medium-grained pentlandite (**Fig. 9.4a**). Owing to their closer proximity to ultramafic boudins, the Birchtree samples are interpreted to be closer in textural character to “primary” magmatic massive sulfides compared to the samples from Thompson.

**Thompson:** The ores in the Thompson mine exhibit a spectrum of textures that vary between the T1 fold nose, the 1C ore body, and the 1D ore body.

T1 ores are SM\$-SED and M\$-SED (**Fig. 9.11a**), but are texturally similar to the Birchtree samples described above. Most are near ultramafic boudins, but some (e.g., JL98-T1-19) occur as concordant massive sulfide lenses hosted by pelitic schists distant from ultramafic boudins. T1 ores typically contain randomly-oriented to oriented, medium- to coarse-grained ultramafic and pelitic inclusions, and contain up to 25% medium- to coarse-grained pentlandite grains (**Fig. 9.11b**). Single crystal inclusions also occur in the T1 massive sulfides; the most abundant crystal inclusions are fine- to medium-grained foliated biotite flakes, and rounded quartz and plagioclase grains.

1C ores are dominantly M\$-SED (**Fig. 9.12a**), but also include M\$-UB, N\$-U, and D\$U. Thompson 1C M\$-SED ores differ from T1 ores in that the pentlandite grains tend to be coarser and distributed into parallel, cm-scale bands within the ore horizons (**Fig. 9.12b**). Single crystals of biotite, quartz, and plagioclase dominate the inclusion population.

1D ores are primarily M\$-SED hosted by pelitic and quartz-rich metasediments that have been intruded by late pegmatitic granite (**Fig. 9.13a**). Because the 1D ore body has

undergone extreme and complex deformation, manifested by undulating contacts between rock units, numerous metre-scale shear zones, and abundant pegmatitic/tonalitic inclusions, 1D ores are unique compared to most other ores in the TNB. The ores in this part of the Thompson mine are interpreted to be relatively more distal to ultramafic boudins than T1 and 1C ore; no interpreted ultramafic parent rocks have been observed within 800 ft along strike of the 1D ore bodies. The ores typically contain up to 40% well-rounded, medium- to coarse-grained pegmatitic/tonalitic inclusions, and up to 10% fine- to medium-grained pentlandite grains (**Fig. 9.13b**). Locally, the pentlandite grains are as coarse-grained as in 1C ores, however, they are interpreted to occur in less deformed portions of the ore body.

**William Lake:** William Lake sulfides are primarily D\$-U and have textures identical to those in other strata-bound disseminated Ni-Cu-(PGE) deposits such as Mt. Keith (Groves & Keays, 1979) and Dumont (Eckstrand, 1975). They occupy interstitial spaces between olivines and occur as very fine ( $\mu\text{m}$ -sized) inclusions in olivine (see Fig. 8.1i). This suggests that these rocks were saturated in sulfide at an early to intermediate stage of their crystallization history (see **Section 8.4.3.5**). Minor M\$-UB and M\$-SED in the William Lake area have macroscopic textures similar to those at Birchtree, T1, and 1C, but are much less deformed than those at 1D.

#### 9.4.4 Textural Variations Across Strike in a Deformed Ore Zone

A detailed investigation of an ore-bearing stratigraphic section in the 1C ore body in the Thompson mine (**Fig. 9.14**) was conducted to assess textural variations of sulfides across and along the strike of a deformed ore zone.

The textures of sulfides across the strike of the 1C ore zone vary with the location of the sulfides in the stratigraphic sequence (**Figure 9.15**: locations A-D). There is a transition from D\$-UM in the interior of the ultramafic body through N\$-U near the margin of the body to M\$-SED along the margin of the body. The transition from D\$-U to N\$-U coincides with increasing serpentinization of the ultramafic host rock, which was likely caused by hydration of the ultramafic body from the exterior to the interior (see discussion in **Chapter 7**).

There is evidence for shearing within M\$-SED at the base of the ultramafic body. Pentlandite porphyroblasts in the ores are flattened and embayed, pyrite aggregates are segregated into mm-scale bands oriented parallel to the foliation of the hosting metasedimentary rocks (**Fig. 9.15**: location E<sub>1</sub>), and the mineralized schists adjacent to the massive sulfides are strongly foliated (**Fig. 9.15**: location F). Further away from the massive sulfide horizon, non-mineralized metasedimentary rocks are less foliated (**Fig. 9.15**: locations G and H).

#### 9.4.5 Textural Variations Along Strike in a Deformed Ore Zone

The textures of M\$-SED in the Thompson 1C section indicate that they have experienced several phases of deformation and metamorphism (**Fig. 9.15**: locations E<sub>1</sub>, E<sub>2</sub>, and E<sub>3</sub>), the history of which is best preserved in pentlandite grains.

For example, elongated and corroded porphyroblasts of pentlandite in location E<sub>1</sub> (**Fig. 9.15**) are flattened parallel to the foliation in the host metasedimentary rocks and are therefore interpreted to have exsolved from *MSS* during retrograde metamorphism ( $< \sim 600^\circ\text{C}$ ) and to have been subsequently deformed. The embayed margins of the porphyroblasts indicate that they reequilibrated with the groundmass and did not completely recrystallize after deformation.

Coarse-grained, equant and chain-textured pentlandite grains in location E<sub>2</sub> (**Fig. 9.15**) contain foliated porphyroblastic mica inclusions (<1mm to 1 cm), suggesting that they exsolved from *MSS* after the sulfides were mobilized away from the ultramafic sill.

Massive sulfides and silicate inclusions at location E<sub>3</sub> (**Fig. 9.15**) are fine-grained, sulfide phases are equigranular and have undulating borders, and mica inclusions are randomly oriented, suggesting that these rocks have undergone cataclasis. However, the equant, equigranular textures of the sulfides suggest that they recrystallized after deformation. Secondary pyrite mimics the textures of pentlandite, and in places appears to be overgrown on pentlandite grains, suggesting that sulfidation occurred after deformation and after exsolution of pentlandite from *MSS*. Pyrite “overgrowths” of this type are common within massive sulfides in the Thompson Mine.

## 9.5 Mineral Chemistry

In order to better constrain the distributions of metals amongst the various minerals, their chemical compositions were determined *in situ* by a combination of wavelength-dispersive X-ray emission spectrometry (WD-XRES) using an electron probe microanalyzer and proton-induced X-ray emission spectrometry (PIXES) using a proton probe microanalyzer. Analytical conditions are described in **Appendix 1** and analytical data are given in **Appendix 5**.

### 9.5.1 Pyrrhotite

The compositions of pyrrhotites in samples from the Thompson, Birchtree, William Lake, Bucko, and Soab North deposits are given in **Appendix 5**. Special care was taken to analyze pyrrhotite grains at least 50 µm away from pentlandite porphyroblasts, in order to avoid grains that may have accumulated Ni via solid-state diffusion (see **Fig. 9.19**).

The compositions of pyrrhotites in the TNB vary both within and between different ore types. Those in disseminated ores contain 36-40 %S, varying systematically with location and rock type, whereas those in semi-massive and massive ores contain 39-40 %S.

An attempt was made to distinguish between monoclinic and hexagonal pyrrhotite on the basis of atomic metal:sulfur (Me/S) ratio, where Me = Fe + Ni + Co. This technique was used by Czamanske et al. (1992) who established Me/S ratios of 0.858-0.883 for monoclinic pyrrhotite, 0.909-0.923 for hexagonal pyrrhotite, and 0.980-1.003 for troilite in Noril'sk-Talnakh ores. However, Kissin (1974) reported a range of 0.898-0.866 for monoclinic pyrrhotite and Arnold (1971) reported a range of 0.899-0.996 for hexagonal pyrrhotite. The Me/S ranges used in this study were 0.86-0.90 for monoclinic pyrrhotite, 0.90-0.99 for hexagonal pyrrhotite, and 0.99-1.000 for troilite. On this basis, the pyrrhotite in the semi-massive and massive sulfides in the 1C ore zone is predominantly monoclinic, whereas the pyrrhotite in disseminated sulfides in the associated ultramafic sill is both hexagonal and monoclinic..

Pyrrhotite in M\$-SED and SM\$-SED is predominantly monoclinic and is enriched in Ni compared to pyrrhotite in D\$-SED (**Fig. 9.22**). Pyrrhotites in M\$-SED range 0.2-1.1 wt% Ni, pyrrhotites in SM\$-SED range 0.3-0.9 wt% Ni, and pyrrhotites in D\$-SED range <0.1-0.8 wt% Ni. Pyrrhotites in D\$-SED that contain 1-5 modal% sulfides and are located less than 1m away from M\$-SED have Ni concentrations that overlap those of M\$-SED and SM\$-SED, suggesting that the Ni contents of disseminated pyrrhotite is a function of proximity to

massive sulfides. Pyrrhotites in M\$-SED at Thompson, William Lake, Bucko Lake, and Soab North all fall within the range 0.2-1.1 wt% Ni (**Fig. 9.23**).

Pyrrhotite in M\$-UB is predominantly monoclinic, but less commonly hexagonal. The monoclinic pyrrhotites at William Lake have higher Ni contents (0.7–0.8 wt% Ni) than those at Thompson and Birchtree (0.1-0.5 wt% Ni: **Fig. 9.24**).

Pyrrhotite in D\$-U is both monoclinic and hexagonal, and exhibits increasing Ni with increasing S (**Fig. 9.25**). The highest Ni contents occur in monoclinic pyrrhotites in the William Lake and Birchtree deposits (predominantly ~0.5 wt% Ni); the lowest Ni contents occur in hexagonal pyrrhotites in the Thompson deposit (generally <0.3 wt% Ni).

Pyrrhotite in D\$-U and M\$-UB at William Lake has higher Ni (generally >0.5 wt% Ni) than that in M\$-SED (generally <0.6 wt% Ni). Pyrrhotite in M\$-UB at Birchtree has lower Ni than that in D\$-U. Pyrrhotite in M\$-SED at Thompson has higher Ni than that in D\$-U.

### 9.5.2 Pentlandite

The compositions of pentlandites in samples from the Thompson, Birchtree, William Lake, Bucko, and Soab North deposits are given in **Appendix 5**. Analyzed pentlandite grains were not categorized in terms of the pentlandite textures (e.g., chains, eyes, or blebs), but were categorized in terms of the rock classification scheme in **Table 9.1** and in terms of the ore body from which they were collected. Flame-textured pentlandite was avoided because of the fine grain size, which resulted in interference from the Fe and Ni in the host pyrrhotite. Special care was also taken to avoid cracks in pentlandite.

Nickel tenors of pentlandites in TNB ores (**Figs. 9.26a, 9.27a, and 9.28a**) show similar trends to the Ni tenors of co-existing pyrrhotites (**Figs. 9.23, 9.24, and 9.25**). Pentlandites in massive sulfides from several TNB deposits have Ni tenors ranging 34-38 wt% Ni (**Fig. 9.26a**). Pentlandites in M\$-UB at William Lake have higher Ni contents (~38 wt% Ni) than pentlandites in similar samples from Thompson and Birchtree (33-35 wt% Ni: **Fig. 9.27a**). Pentlandites in D\$-U at William Lake and Birchtree are characterized by high Ni contents (35-38 wt% Ni) in comparison to similar samples from Thompson T1 (33-35 wt% Ni) or Thompson 1C (31-33 wt% Ni) (**Fig. 9.28a**). Pyrrhotites co-existing with pentlandite in D\$-U at William Lake and Birchtree also have high Ni contents (~0.5 wt% Ni) compared to pyrrhotites in D\$-U at Thompson T1 and 1C (<0.3 wt% Ni) (**Fig. 9.25**).

Thus, the Ni contents of pentlandites in D\$-U, M\$-UB, and M\$-SED, pyrrhotites in D\$-U (**Section 9.4.1**), and relict igneous olivines (**Section 8.3.4**) at William Lake are *all* enriched in Ni relative to similar phases in other areas of the TNB. In contrast, pentlandites in M\$-UB at Birchtree have *lower* Ni contents than those in D\$-U in the same area, and pentlandites in D\$-SED and M\$-SED in Thompson have *higher* Ni contents than those in D\$-U in the same area.

These differences are also evident in the Ni/Co ratios of pentlandite. As discussed in **Section 9.16**, Thompson pentlandites that were subjected to higher degrees of deformation have slightly higher Ni contents and much lower Co contents, and therefore higher Ni/Co ratios than less deformed counterparts. M\$ at Thompson 1D and Bucko Lake have the highest Ni/Co ratios among the TNB deposits (>100: **Fig. 9.26b**). Given that the Ni concentrations in the pentlandites at 1D ore body and Bucko Lake are within the same range as the other deposits (**Fig. 9.26a**), the high Ni/Co ratios can be attributed to lower Co abundances in the



two deposits. The lower Co abundances probably do not reflect an initially low magmatic Co concentration, as associated pyrite is enriched in Co, so they probably reflect redistribution during deformation of the Thompson 1D and Bucko ore bodies (the host rocks at Bucko are Ospwagan Group paragneisses that were previously interpreted as Archean gneisses).

Pentlandites in M\$-UB at William Lake are characterized by higher Ni/Co ratios (~100 to 200) than similar samples from the Birchtree and Thompson deposits (<100: **Fig. 9.27a**), which is clearly related to lower Co contents (**Fig. 9.27b**), not higher Ni contents. However, the higher Ni contents of pentlandites in D\$-U at William Lake (**Fig. 9.28a**) means that they have Ni/Co ratios that fall within the range of Thompson pentlandites (35 to 80: **Fig. 9.28b**). Pentlandites in M\$-UB at the Thompson mine (**Fig. 9.27**) have Ni/Co ratios and Ni contents that are markedly lower than those in M\$-SED (**Fig. 9.26**).

Pentlandite in D\$-U, M\$-UB, and M\$-SED at Birchtree have the lowest Ni/Co ratios of all sampled ore bodies (<40: **Figs. 9.26b, 9.27b, and 9.28b**), which are attributable to the higher Co contents of pentlandite at Birchtree (1.0 to 3.3 wt% Co) compared to the other sampled ore bodies (typically <1.0 wt% Co: **Appendix 5**). The higher Co values in all of the sulfide ore types at the Birchtree deposit may reflect a different primary magma composition, a different R factor, and/or greater modification during deformation and metamorphism. The latter process would account for the narrow range in Ni/Co ratios in Birchtree pentlandites, which may reflect a greater degree of homogenization accompanying greater degrees of deformation and/or metamorphism.

### 9.5.3 Trace Elements

Trace element analyses of sulfide minerals in 33 thin sections of samples from the Thompson (1C and 1D ore bodies), Birchtree, and William Lake deposits are given in **Appendix 6**. The results may be summarized as follows:

- 1) Zinc is concentrated in chalcopyrite (47-505 ppm Zn).
- 2) Arsenic is concentrated in secondary subhedral to euhedral pyrite grains within massive sulfide ores (M\$-UB, SM\$-SED, M\$-SED). Secondary pyrite containing up to 409 ppm As occurs with paragenetically-late gersdorffite (NiAsS) in Thompson ores, suggesting that As and S were introduced into the ores during the late stages of deformation and metamorphism.
- 3) Secondary pyrite grains contain significant amounts of Co (up to 1.4%).
- 4) The abundances of PGEs in the sulfide minerals are below the detection limits of the PIXE method (<4-8 ppm Ru, Rh, and Pd; <14-65 ppm Os, Ir, Pt, and Au).
- 5) There is a positive correlation between Ni and Se in both pyrrhotite and pentlandite in TNB massive sulfide ores (**Figs. 9.29 and 9.30**). Pentlandite and pyrrhotite within massive sulfide ores from the Thompson 1D ore body have higher Se contents than similar samples from Birchtree, Thompson 1C, and William Lake (**Figs. 9.29 and 9.30**).

The similar abundances of Se in pyrrhotite and pentlandite (**Figs. 9.29 and 9.30**) suggests that Se does not preferentially partition into either phase. The higher Se contents of sulfides in the 1D ore body sulfide minerals may reflect a primary magmatic Se signature or addition of Se during deformation and metamorphism.

#### 9.5.4 Variably Deformed Sulfide Minerals

The sulfides in the massive ore horizon studied in the Thompson 1C ore body (**Fig. 9.14**) appear to exhibit systematic changes in chemical composition with progressively higher degrees of deformation (i.e., from location  $E_1$  to  $E_3$ ). The relative abundances of Fe, Ni, and Co in pentlandite in the Thompson 1C ore body are shown in **Figure 9.16**. With increasing degree of deformation of the massive sulfides, there is a ~70% *decrease* in the Co content of pentlandite, a ~25% *increase* in the Co content of pyrrhotite, a ~15% *increase* in the Co content of pyrite, a ~3% *increase* in the Ni content of pentlandite, a ~20% *decrease* in the Ni content of pyrrhotite, and a ~90% *decrease* in the Ni content of pyrite (**Table 9.2**). Thus, the Ni/Co ratios of more deformed pentlandite in location  $E_3$  are ~250% higher than those of less deformed pentlandites in location  $E_1$  (**Table 9.2**). Conversely, the Ni/Co ratios of equant recrystallized pyrites in location  $E_3$  are ~90% lower than those of foliated pyrite aggregates in location  $E_1$  (**Table 9.2**). The limited number of samples and uncertainties regarding whether they represent progressive deformation of precisely the same protolith preclude precise mass balance calculations, but regardless of whether metals were introduced or lost, the mineral chemical data indicate that Co moved out of pentlandite and into pyrite and that Ni moved out of pyrite and pyrrhotite and into pentlandite during that during deformation and sulfidation. Co commonly substitutes for Fe in the pyrite lattice (Loftus-Hills et al., 1971; Huston et al., 1995). The Ni content of pentlandite varies with the Ni content of the bulk sulfide, increasing with increasing Ni content in Po-Pn, Po-Pn-Py, Py-Pn, Py-Ml-Pn, Pn-Ml, and Pn-Hz assemblages (Misra & Fleet, 1974).

The relative abundances of Fe, Ni, and S in pentlandite in the Thompson 1C ore body are shown in **Figure 9.17**. The Ni contents of pentlandite increase systematically with increasing serpentinization of the ultramafic host rock (reflecting uptake of Ni from olivine: Eckstrand, 1975; Donaldson, 1981) and with increasing degree of deformation of the massive sulfide ore (as discussed above). There is a complementary increase in Ni concentration in pyrrhotite co-existing with pentlandite (**Fig. 9.18**), indicating that equilibrium was broadly maintained between pentlandite and pyrrhotite.

In Thompson 1C ores, pyrite occurs proximal to the ultramafic sill as aggregates that are oriented parallel to the stress-induced foliation (**Fig. 9.15**,  $E_1$ ). The pyrite could have formed via addition of S or oxidation of pyrrhotite. The absence of magnetite occurring with the sulfides suggests that oxidation was not a dominant process, and that the pyrite most likely formed by sulfidization of pyrrhotite. The distribution of pyrite along the foliation suggests that S may be been mobilized into the ores by fluids migrating along the foliation. The embayed nature of the sheared pentlandite grains (**Figure 9.15**,  $E_1$ ), as well as the pyrite-poor halo around the pentlandite grains (**Fig. 9.15**,  $E_1$ ), suggests that both Ni and S were mobilized from the massive ore proximal to the ultramafic sill. These observations support the suggestion that fluid-assisted mobilization of metals may occur in massive sulfide deposits (see discussion by Marshall et al., 2000).

#### 9.5.5 Metal Diffusion

Solid-state diffusion of metals can occur on a microscopic scale during re-equilibration of massive sulfides cooling from high temperatures (Klotsman et al., 1963; Condit et al., 1974; Ewers, 1972; see also Naldrett et al., 1967; McQueen, 1979). For example, Fe has a self-diffusion coefficient of  $\sim 10^{-9}$  cm<sup>2</sup> sec<sup>-1</sup> in pyrrhotite at 480°C and Ni has a self-diffusion coefficient of  $\sim 10^{-8}$  cm<sup>2</sup> sec<sup>-1</sup> in nickel monosulfide at 720°C. These diffusion rates (~18m

per m.y. and ~56m per m.y., respectively) are high enough to be significant during the ~14-21 Ma time scale estimated for polyphase regional metamorphism in different locations within the TNB (**Section 10.4**), especially given that diffusion rates in ores undergoing deformation would be much higher.

**Table 9.2.** Compositions of sulfide minerals in samples from the Thompson 1C ore body.

Location	Sample Number	Mineral	S (wt%)	Fe (wt%)	Co (wt%)	Ni (wt%)	Ni/Co
E1	DM98-1C-07	Pn	33.2	31.2	0.41	35.1	85
	DM98-1C-07	Pn	33.3	31.3	0.47	34.9	75
	DM98-1C-07	Pn	33.0	30.7	0.39	35.7	91
	average		33.2	31.1	0.42	35.2	84
	DM98-1C-07	Po	39.3	60.4	0.04	0.27	6.7
	DM98-1C-07	Po	39.3	60.2	0.03	0.32	13
	DM98-1C-07	Po	39.1	60.5	0.05	0.40	7.8
	average		39.2	60.4	0.04	0.33	9.1
	DM98-1C-07	Py	53.1	45.8	0.64	0.35	0.56
	DM98-1C-07	Py	52.8	45.5	0.77	0.86	1.1
	DM98-1C-07	Py	52.8	44.8	1.90	0.42	0.22
	average		52.9	45.4	1.10	0.54	0.63
	JL98-1C-20	Pn	33.1	30.6	0.14	36.0	251
	JL98-1C-20	Pn	32.9	30.5	0.12	36.4	314
	JL98-1C-20	Pn	32.9	30.5	0.12	36.3	301
	average		33.0	30.5	0.13	36.2	289
E3	JL98-1C-20	Po	39.5	60.1	0.06	0.25	4.2
	JL98-1C-20	Po	39.4	60.3	0.06	0.24	3.7
	JL98-1C-20	Po	39.5	60.1	0.02	0.32	15
	average		39.5	60.2	0.05	0.27	7.6
	JL98-1C-20	Py	53.0	45.9	0.93	0.05	0.06
	JL98-1C-20	Py	52.9	45.5	1.48	0.03	0.02
	JL98-1C-20	Py	52.9	45.6	1.48	0.05	0.03
	average		52.9	45.6	1.29	0.04	0.04

Compositions determined by wavelength-dispersive X-ray emission spectrometry using the electron probe microanalyzer at the University of Manitoba. Analytical methods described in **Appendix 1**. Abbreviations: Pn = pentlandite, Po = pyrrhotite, Py = pyrite. Relative locations of samples shown in **Figure 5.16**.

Electron microprobe analyses across an equant pentlandite porphyroblast and adjacent pyrrhotite in a M\$-SED horizon at Thompson indicate that the Ni content of pyrrhotite increases from a background of ~0.2 wt% Ni to a maximum of ~0.6 wt% Ni within 50  $\mu$ m of the pentlandite porphyroblast (**Fig. 9.19**). The data are not precise enough to determine whether the profiles have a form consistent with diffusion (Crank, 1980), but suggest that solid-state diffusion of Ni occurred during post-metamorphic cooling and re-equilibration of the sulfides.

Ni contents of pentlandite and pyrrhotite in the Thompson 1C ultramafic body increase from the interior to the exterior of the body (**Figs. 9.16, 9.17, and 9.18**). However, this coincides with an increase in the degree of serpentinization of the ultramafic rock and is almost certainly attributable to release of Ni from olivine during serpentinization and subsequent incorporation of Ni into sulfides (Eckstrand, 1975; Groves & Keays, 1979; Donaldson, 1981).

Samples taken across the Thompson 1C ultramafic body into adjacent M\$-UB and metasediments (illustrated schematically as section I-I' in **Fig. 9.14**) and across an M\$-UB body enclosed in metasediments (illustrated schematically as section J-J' in **Fig. 9.14**) indicates that the Ni contents of pyrrhotites and pentlandites in M\$-UB and M\$-SED within ~20m of the ultramafic body are significantly higher than those disseminated in the ultramafic rock or in metasediments distant from the ultramafic body (**Figs. 9.20 and 9.21**). This relationship is the reverse of what is normally observed in most magmatic sulfide deposits, in which disseminated sulfides normally have higher Ni tenors because they equilibrated with larger amounts of silicate magma (see discussion by Lesher and Campbell, 1993) and/or have been upgraded during serpentinization (see above). There are three possible explanations for these relationships: 1) S has been added to the ultramafic rocks, converting magnetite (derived via serpentinization of olivine) into pyrrhotite, reducing the Ni tenor of the small amount of magmatic sulfides (and therefore reducing the Ni contents of pyrrhotite and pentlandite), 2) Ni has been mobilized *en masse* from the ultramafic rocks into M\$-UB and adjacent M\$-SED, and/or 3) Ni has been introduced into M\$-UB and adjacent M\$-SED from sources external to the sampled ore zone. Petrographic observations (e.g., paucity of pyrite) and whole-rock Ni<sub>100</sub> contents that are within the normal magmatic range suggesting that the low Ni contents of pyrrhotite and pentlandite in the ultramafic rocks are *not* attributable to addition of S. The whole-rock Ni contents of the ultramafic rocks are broadly similar to non-mineralized ultramafic rocks in the TNB (900-3500 ppm Ni for 20 – 48 wt% MgO: **Section 8.4.4.1**) suggesting that Ni has not been lost *en masse* from the ultramafic rocks. Thus, it seems unnecessary for Ni to have been added to M\$-UB and adjacent M\$-SED from external sources.

The relationship between the concentration of Ni in pyrrhotite and its hexagonal or monoclinic character is not entirely clear from the sections in **Figures 9.20 and 9.21**; however, monoclinic pyrrhotite dominates over hexagonal pyrrhotite within the massive sulfide horizons and within metasedimentary rocks nearest to the massive sulfide horizons.

Ni enrichment in pyrrhotite (>0.2 wt% Ni) coincides with a Ni enrichment in co-existing pentlandite grains (**Fig. 9.20**). The Ni enrichment in pyrrhotite also coincides with increasing modal percentage of pentlandite. Importantly, pentlandite in disseminated metasedimentary sulfides is always associated with Ni-enriched pyrrhotite and only occurs proximal to ore zones (within ~20m). Therefore, the Ni enrichment around the horizon is interpreted to be a local phenomenon. The observed Ni halo suggests that Ni migrated away from the massive sulfide horizon and entered sulfide blebs within the metasedimentary rocks, either via solid-state diffusion or with the assistance of fluids. The presence of fluids is likely given that the ultramafic rocks are serpentinized and the massive sulfides have been sulfidated.

## 9.6 Whole Rock Chemistry

### 9.6.1 Normalization to 100% Sulfides

In order to compare the metal concentrations in samples with widely varying sulfide contents, it is necessary to recalculate the metal abundances to 100% sulfides (e.g., Naldrett, 1989). As noted above, the normalization technique utilized here assumes that all of the base and precious metals are housed in sulfides and that the sulfide assemblage comprises monoclinic pyrrhotite [Fe<sub>0.875</sub>S], pentlandite [Fe<sub>4.3</sub>Ni<sub>4.7</sub>S<sub>8</sub>], and stoichiometric chalcopyrite

[CuFeS<sub>2</sub>]. The Thompson 1D massive ores generally have higher Ni<sub>100</sub> contents than Birchtree or Pipe ores (**Fig. 9.31**).

### 9.6.2 Ni/Co Ratios

Ni/Co ratios of ultramafic rocks associated with the Thompson, Birchtree, and Pipe massive ores are very similar (generally 20-25: **Fig. 9.32**). However, massive sulfides at the Thompson 1D ore body have higher Ni/Co ratios (24-113) than those at Birchtree (6-64) and Pipe (20-32) (**Fig. 9.33**). Because  $D_{Ni}^{Sul/Ol}$  is of the order of 50-150, depending on  $fO_2$ , whereas  $D_{Co}^{Sul/Ol}$  is of the order of 35, the Ni/Co ratios of sulfides formed at high D or low should be greater than those of associated olivine cumulate rocks. However, because  $D_{Ni}^{Sul/Ol}$  and  $D_{Co}^{Sul/Ol}$  are normally  $> R/10$ , they are markedly influenced differently by the sulfide:silicate mass ratio (see below): they approach the Ni/Co ratio of olivine at very low R, but approach a ratio equal to that of the olivine times the ratio between the two Ds at very high R. Thus, the Ni/Co ratios of Thompson ores are consistent with having formed at a higher R than those at Birchtree or Pipe, as concluded long ago by Naldrett et al. (1979).

### 9.6.3 $\delta^{34}S$ and S/Se Ratios

<sup>32</sup>S and <sup>34</sup>S fractionate differently into different S-bearing phases with the degree of fractionation with the degree of fractionation decreasing with increasing temperature (Faure, 1986). S isotopic fractionations are normally expressed as the per mil deviation in the ratio of the heavier <sup>34</sup>S isotope to that of the lighter <sup>32</sup>S isotope normalized to the <sup>34</sup>S/<sup>32</sup>S ratio of the Canon Diablo meteorite,  $\text{‰}\delta^{34}S_{CDT}$ , where:

$$\text{‰}\delta^{34}S_{CDT} = 1000 * ({}^{34}S/{}^{32}S_{\text{sample}} - {}^{34}S/{}^{32}S_{CDT}) / {}^{34}S/{}^{32}S_{CDT}$$

Se and S also fractionate differently into different S-bearing phases and is often used as a proxy for S isotopic variations. S is orders of magnitude more abundant than Se, so most authorities (e.g., Stanton, 1972) express S and Se fractionations in terms of S/Se ratios. However, Eckstrand et al. (1989) used  $10^6 * \text{Se/S}$  ratios, a convention adopted by Liwanag (2001) and used in several of figures in this Chapter.

Eckstrand et al. (1989) showed that S/Se ratios of Thompson ores (5900-35700 S/Se, 169-27  $10^6 * \text{Se/S}$ ) vary between those of the barren sulfide-facies iron-formations (12800-35700 S/Se, 78-27  $10^6 * \text{Se/S}$ ) and the mantle (2900-4400 S/Se, 345-227  $10^6 * \text{Se/S}$ ; see **Fig. 9.34**), suggesting that the ores were generated by melting of the associated sulfide-facies iron-formations, like most other deposits of this type (Leshner, 1989).

S/Se ratios for massive and semi-massive sulfide samples from this study are consistent with there being a large sedimentary sulfide component in the ores of the Thompson 1D ore body, Birchtree Mine, and Pipe 2 deposit ( $>8300$  S/Se,  $120$   $10^6 * \text{Se/S}$ ; **Fig. 9.35**). Thompson massive ores have slightly lower S/Se ratios ( $\sim 16700$  S/Se,  $\sim 60$   $10^6 * \text{Se/S}$ ) than Birchtree and Pipe 2 ores ( $\sim 25000$ ), although there is considerable overlap in the Se/S values. The lower S/Se (higher  $10^6 * \text{Se/S}$ ) ratios of the Thompson ores suggests that they formed at higher R factors than those at Birchtree and Pipe.

The S/Se ratios of ultramafic rocks associated with the same massive ores are shown in **Figure 9.36**. The similarity in S/Se ratios of the ores at Thompson, Birchtree, and Pipe with those of the associated ultramafic rocks indicate that the host rocks in those areas have also been contaminated by crustal sulfides and are consistent with a magmatic (rather than

hydrothermal) origin for the ores. The S/Se ratios of William Lake ultramafic rocks (4200-25000 S/Se,  $40 \cdot 10^6 \text{ Se/S}$ ) extend to higher values than those at Birchtree, Pipe, and Thompson (7700-100000 S/Se,  $130 \cdot 10^6 \text{ Se/S}$ ), suggesting that the William Lake ultramafic rocks (and ores) formed under higher R conditions than those at Birchtree, Pipe, and Thompson.

#### 9.6.4 Platinum Group Elements (PGEs)

Chondrite-normalized chalcophile-element plots of the Thompson and Birchtree massive and semi-massive ores analyzed in this study indicate that the samples are slightly enriched in Cu and PPGE relative to Ni and IPGE, as expected for derivation from a magma derived by moderately high degree partial melting of the mantle (Naldrett & Barnes, 1986), but that they are significantly depleted in Pt relative to PGEs of similar compatibility (**Fig. 9.37**). This Pt depletion is also evident in ores from the Pipe deposit analyzed by Naldrett et al. (1979) and in ores from the Pipe II and Thompson deposits analyzed by Bleeker (1990b). Because Pt has a compatibility intermediate between that of Pd and Rh, the mantle-normalized concentration of Pt should be intermediate between the mantle-normalized concentrations of Pd and Rh. Thus, the magnitude of the Pt depletion can be expressed as a ratio of the observed concentration (ave. 41.6 ppb) to that of the expected concentration (ave. 125.8 ppb) derived by interpolation between Pd and Rh:

$$\text{Pt/Pt}^* = 41.6 \text{ ppb} / 125.8 \text{ ppb} = 0.33$$

or as a relative depletion:

$$\Delta\text{Pt} = 100 * (41.6 \text{ ppb} - 125.8 \text{ ppb}) / 41.6 \text{ ppb} = -202\%$$

Chondrite-normalized plots of a wide range of ore samples from Birchtree, Thompson, and Pipe (**Fig. 9.38, 9.39, and 9.40**, respectively) indicate that negative Pt anomalies occur only in M\$. D\$ and N\$ in these localities do not exhibit negative Pt anomalies.

Thompson 1D ores have higher Pd/Pt ratios (ave. 93: **Table 9.3**) than Thompson 1C ores (ave. 30), Thompson T1 ores (ave. 51), or Birchtree ores (ave. 24). Although the sulfides in the 1D ore body have undergone extensive brittle deformation and are also enriched in semi-metals (see below), they also have higher Pd/Ir ratios (ave. 18) than 1C ores (ave. 3.8), T1 ores (ave. 5.5), and Birchtree ores (ave. 1.7). This suggests that the PGE fractionation reflects a magmatic rather than metamorphic process.

#### 9.6.5 Trace Elements

Thompson 1D ores have As, Bi, and Pd contents that are an order of magnitude higher than those at Thompson 1C, Thompson T1 fold nose, and Birchtree (**Table 9.4**). For example, As contents of 1D ores range 411-510 ppm, compared to 34-97 ppm in 1C ores, 13-114 ppm in T1 ores, and 8-96 ppm in Birchtree ores. The elevated As contents of the 1D samples correlates with the presence of paragenetically late pyrite, which can contain up to 400 ppm As (**Appendix 6**), and the presence of euhedral to subhedral grains of gersdorffite (NiAsS). Niccolite (NiAs) also rarely occurs in Thompson ores (e.g., sample T119 from the T1 Mine).

**Table 9.3.** Chalcophile element and PGE data for massive and semi-massive sulfides in the TNB

	Ore	Ni <sub>100</sub>	Co <sub>100</sub>	Ir <sub>100</sub>	Ru <sub>100</sub>	Rh <sub>100</sub>	Pt <sub>100</sub>	Pd <sub>100</sub>	Au <sub>100</sub>	Cu <sub>100</sub>	S <sub>100</sub>							
Sample	Type	(wt%)	(wt%)	(ppb)	(ppb)	(ppb)	(ppb)	(ppb)	(ppb)	(wt%)	(wt%)	Pd/Ir	Pd/Pt	Ni/Co	Ni/Cu	Pd/Rh	Pd/Ir av	Pd/Pt av
<b>Thompson 1C ore body</b>																		
JL98-1C-19A	SM\$-SED	8.57	0.15	129	421	137	9	259	4	0.29	33.3	2.00	29.3	56.2	29.3	1.89	3.83	30.3
JL98-1C-20	M\$-SED	8.40	0.11	144	468	134	8	298	14	0.06	37.3	2.07	37.4	76.8	131	2.22		
JL98-1C-25A	M\$-SED	7.36	0.15	180	477	158	25	693	11	0.37	34.6	3.85	27.8	50.3	19.7	4.39		
JL98-1C-25B	M\$-SED	7.53	0.17	157	451	160	33	765	21	0.35	33.6	4.87	23.4	44.3	21.8	4.78		
JL98-1C-25D	M\$-SED	9.22	0.21	154	477	166	29	977	16	0.33	35.5	6.36	33.5	44.2	28.1	5.89		
<b>Thompson 1D ore body</b>																		
JL98-1D-07	M\$-SED	11.4	0.20	102	127	148	9	1799	36	0.33	39.9	17.7	197	57.8	34.8	12.2	17.90	92.9
JL98-1D-14	SM\$-SED	12.0	0.17	53	294	128	11	1162	55	0.35	33.8	22.1	102	70.9	34.0	9.08		
JL98-1D-18A	SM\$-SED	11.5	0.10	156	249	186	494	2173	131	0.12	27.4	13.9	4.40	113	98.2	11.7		
JL98-1D-20	SM\$-SED	13.5	0.16	67	115	108	18	1199	34	0.22	31.5	17.9	67.8	86.2	62.0	11.1		
<b>Thompson T1 mine</b>																		
JL98-T1-09A	M\$-UB	7.98	0.18	4	4	38	5	395	10	0.28	38.2	100	77.1	44.8	28.4	10.4	5.47	51.5
JL98-T1-12	M\$-UB	7.10	0.15	24	38	29	2	140	1	0.21	37.9	5.87	83.0	46.2	34.2	4.83	(n=3)	
JL98-T1-19	M\$-SED	5.81	0.10	121	408	143	32	622	57	0.04	35.0	5.13	19.5	55.4	152.8	4.35		
JL99-T1-35	M\$-SED	0.85	0.12	174	489	220	36	942	19	0.28	35.5	5.41	26.2	7.01	3.06	4.28		
<b>Birchtree Mine</b>																		
JL98-BT-02	M\$-UB	5.11	0.21	60	154	28	27	92	22	0.06	37.3	1.54	3.35	24.2	83.8	3.29	1.69	24.2
JL98-BT-10	M\$-SED	4.35	0.18	12	49	10	1	20	0	0.04	37.7	1.64	32.3	23.8	99.3	2.00		
JL98-BT-15	M\$-SED	5.85	0.21	65	169	32	3	143	5	0.12	33.3	2.20	49.6	27.7	50.1	4.47		
JL98-BT-16B	M\$-UB	5.17	0.16	37	115	25	3	61	1694	0.91	32.6	1.65	22.6	31.9	5.67	2.44		
JL98-BT-20	M\$-UB	5.07	0.20	52	147	38	6	74	14	0.16	37.0	1.42	13.3	25.5	31.6	1.95		

All values recalculated to 100% sulfides (see discussion in text).

**Table 9.4.** Trace element data for massive and semi-massive sulfides from the TNB.

Sample	Ore Type	S (wt%)	Se (ppm)	S/Se	As (ppm)	Bi (ppm)
<b>Thompson 1C</b>						
JL98-1C-19A	SM\$-SED	33.3	25.2	13214	34	1
JL98-1C-20	M\$-SED	37.3	24.5	15224	44	3
JL98-1C-25A	M\$-SED	34.6	31.1	11125	84	4
JL98-1C-25B	M\$-SED	33.6	27.6	12174	97	4
JL98-1C-25D	M\$-SED	35.5	32.2	11025	86	5
<b>Thompson 1D</b>						
JL98-1D-07	M\$-SED	39.9	42.2	9455	425	41
JL98-1D-14	SM\$-SED	33.8	31.5	10730	323	35
JL98-1D-18A	SM\$-SED	27.4	26.6	10301	264	–
JL98-1D-20	SM\$-SED	31.5	22.6	13938	321	28
<b>Thompson T1</b>						
JL98-T1-09A	M\$-UB	38.2	22.2	17207	13	5
JL98-T1-12	M\$-UB	37.9	34.3	11050	87	4
JL98-T1-19	M\$-SED	35.0	24.4	14344	114	6
JL99-T1-35	M\$-SED	35.5	32.0	11094	108	–
<b>Birchtree Mine</b>						
JL98-BT-02	M\$-UB	37.3	22.3	16726	49	1
JL98-BT-10	M\$-SED	37.7	19.0	19842	34	<1
JL98-BT-15	M\$-SED	33.3	23.0	14478	71	2
JL98-BT-16B	M\$-UB	32.6	15.7	20764	96	–
JL98-BT-20	M\$-UB	37.0	17.4	21264	82	2

There is a positive correlation between Bi and Pd in Thompson and Birchtree massive sulfide ores (**Fig. 9.41**). Bismuth contents are much higher in 1D ores (28-41 ppm) than in 1C ores (1-5 ppm), T1 ores (4-6 ppm), and Birchtree ores (<2 ppm). Palladium contents are also much higher in 1D ores (1162-2173 ppb) than in 1C ores (259-977 ppb), T1 ores (140-942 ppb), and Birchtree ores (20-143 ppb). The elevated abundances of Bi and Pd in the 1D ores can largely be attributed to late-stage Pd-bearing bismuthotellurides (**Fig. 9.42**). They are typically associated with pentlandite, sometimes with euhedral gersdorffite (**Fig. 9.42c**), but are also hosted by pyrrhotite.

There are positive correlations between Ni and As (**Fig. 9.43**), Ni and Pd (**Fig. 9.44**), and to a lesser extent Ni and Bi (**Fig. 9.45**), in Thompson 1D, Birchtree, and Pipe 2 massive sulfides. This suggests that the same processes which concentrated As, Pd, and Bi in these ores may have also concentrated Ni.

#### 9.6.6 Comparison with Kambalda and Langmuir

**Thompson:** Type V ores in the TNB are variably depleted in PPGE relative to IPGE (**Figs. 9.49a,b**), reflecting variably low R factors (Naldrett et al., 1979). They are strongly enriched in As and Mo compared to Kambalda ores. These are not particularly abundant elements in the associated barren sulfide facies iron-formations (**Figs. 9.49 a,b**), suggesting that they have interacted with crustally-derived metamorphic fluids. Type IVa Ni-enriched metasedimentary ores in the TNB are moderately depleted in Cr and Ir (**Fig. 9.49a**),



suggesting that they have been upgraded via solid-state diffusional rather than hydrothermal or tectonic processes (Leshner & Keays, 2002).

**Kambalda:** Average Type I ores at Kambalda exhibit moderately fractionated mantle-normalized metal distribution patterns with  $S \sim Pt > Te > Pb > Pd \sim Bi \sim Se \sim Au > Ru > Cu > As > Os > Ir \sim Rh \sim Ni \sim Mo > Co > Fe > Zn \sim Re > Cr > Ag$  (**Fig. 9.48c**). The ores at Edwards Lode (Heath et al., 2001) are strongly enriched in As and strongly depleted in Zn and Cr compared to normal Kambalda ores (**Fig. 9.49c**), suggesting that they have been hydrothermally and metamorphically modified. The footwall stringers that have been analyzed at Kambalda are slightly enriched in Cu and to a lesser extent Au relative to Pd, Ni, and Ir (**Fig. 9.49c**, FW stringer), suggesting that they are mechanically-mobilized massive sulfides (Type V) or early magmatic veins rather than late fractionated sulfide liquids. Type IVb sulfides in hydrothermal quartz veins at Kambalda (**Fig. 9.49c**, HQV) have broadly similar Au, Ni, and Fe contents as average Type I sulfides, but are slightly enriched in Se, slightly depleted in Pd, Cu, and Zn, and *strongly* depleted in Ir and Cr, consistent with hydrothermal transport and deposition (Keays et al., 1982; Leshner & Keays, 1984; 2002). Type IVa Ni-enriched metasedimentary ores at Kambalda (**Fig. 9.49c**, Ni-SED) have broadly similar Pd, Au, Cu, and Fe contents as average Type I ores, but are strongly enriched in Se, As, Zn, and Ag, slightly depleted in Ni, Co, and Cr, and moderately depleted in Ir, suggesting that they have been upgraded via solid-state diffusional and tectonic rather than hydrothermal processes (Leshner & Keays, 1984, 2002; Paterson et al., 1984).

## 9.7 Interpretations

### 9.7.1 Metamorphic Textures

Thompson, Birchtree, and William Lake massive ores (M\$-UB and M\$-SED) exhibit abundant textural evidence of metamorphic modification. In the Thompson mine, particularly in the 1C ore body, massive sulfide horizons that occur both proximal and distal to ultramafic sills commonly consist of coarse-grained equant to ovoid pyrrhotite and pentlandite that are segregated into cm-scale bands (e.g. **Fig. 9.12b**). Massive Fe-Ni sulfide ores that have undergone amphibolite facies metamorphism commonly exhibit layered fabrics defined by the segregation of pentlandite, pyrrhotite, and pyrite into mm- to cm-scale bands (Barrett et al., 1977; McQueen, 1979; Marston & Kay, 1980; Barnes & Hill, 2000). The phase equilibria in the Fe-Ni-Cu-S system vary with T and composition, particularly S and Ni content (Naldrett et al., 1967; Craig and Kullerud, 1969; Misra and Fleet, 1974; Hill, 1984) and some banding could have been preserved in particularly S-rich or Ni-rich ores at lower T (see discussion by McQueen, 1979), however, under the middle-upper amphibolite facies metamorphic conditions experienced by most of the ores in the TNB, they should have reverted to *MSS* plus oxides (magnetite, ferrochromite) during metamorphism. Thus, most of the banding was probably produced during retrograde metamorphism by crystallization of pyrrhotite, pentlandite, and pyrite from *MSS* following cooling below 500-600°C. The mesoscopic fabrics of the ores, defined by folded and sheared trains of oriented inclusions, indicate that deformation continued during retrograde metamorphism, and the equant nature of individual sulfide phases reflects annealing and recrystallization at lower temperatures.

The concentration of chalcopyrite along contacts between massive sulfide horizons and adjacent metasedimentary rocks may reflect magmatic fractionation (Hawley, 1965; Ebel & Naldrett, 1996) and/or physical migration of more ductile chalcopyrite during metamorphism

(Kelly and Clark, 1975; see also Barrett et al., 1977). The pyrite-chalcopyrite symplectites in TNB massive ores may represent chalcopyrite-rich areas of the ore that reverted to pyrite plus intermediate solid-solution (*ISS*) or a Cu-rich *ISS* that exsolved out of metamorphic *MSS*; chalcopyrite may have then been reformed by the reaction of *ISS* with pyrite at lower, post-metamorphic temperatures (Craig & Kullerud, 1969; see also Barrett et al., 1977).

The presence of euhedral to subhedral gersdorffite and pyrite associated with annealed pentlandite and pyrrhotite indicates that gersdorffite and pyrite crystallized late in the paragenetic sequence, suggesting that semi-metals and PGEs are more soluble in *MSS* and/or semi-metals and PGEs were added during metamorphism.

### 9.7.2 Magmatic Processes

The main factors affecting the compositions of Ni-Cu-(PGE) sulfide ores during magmatic processes are:

- 1) The composition of parental magma, which depends on the composition, mineralogy, and degree of partial melting of the source
- 2) The degree of fractionation of any Ni-, Co- and/or PGE-bearing minerals (e.g., olivine, chromite or discrete PGMs) from the magma
- 3) The relative mass of sulfide with which the silicate magma interacts (R factor)
- 4) Any metal contributions from the country rocks
- 5) The degree of fractionation crystallization of the sulfide liquid, resulting in the removal of Cu-poor *MSS* and enrichment the remaining sulfide liquid in Cu and PPGE

Whereas factors 1 and 2 may be constrained relatively well from the whole-rock compositions of the mafic and ultramafic rocks associated with the ores (see **Chapter 8**), the effects of factors 3 to 5 are still poorly constrained for many of the deposits in the TNB. However, as a result of the large amount of data compiled for the ores during the current and previous projects that investigated the sulfide mineralization of the TNB, it is possible to examine the effect of each of these processes in turn. Although much of the variation may be accounted for by magmatic processes, many chemical and textural features of the ores (as discussed in **Sections 9.2 and 9.3**) indicate that their compositions have also been substantially effected by metasomatism and element mobility during deformation.

#### 9.7.2.1 Chalcophile Element Composition of Parental Magma

If it assumed that the sulfide ores formed as a result of the interaction of an ultramafic magma with a externally-derived sulfide melt, then any modelling or discussion of the whole-rock compositions of ores depends very strongly on the estimated initial composition of the magma. Although the compositions of the magma must have varied from deposit to deposit as a result of different degrees of fractional crystallization during emplacement, the parental composition of the magma can be deduced from the whole-rock major and minor element compositions of the ultramafic bodies and mafic volcanic rocks of the TNB (**Section 8.2**), focussing on least-unaltered, sulfide-poor, aphyric mafic or ultramafic magmas that would could have been in equilibrium with the most magnesian cumulate olivines in the ultramafic bodies (Fo<sub>91-93</sub>; **Section 8.3.2**).

Although it was suggested in **Sections 8.2** and **8.3** that the volcanic rocks of the Bah Lake Formation and the parental magmas to the ultramafic bodies were probably unrelated owing to differences in both their major and trace element compositions (resulting from difference in either their source regions and/or contamination during emplacement), if the two magmas formed by similar degrees of partial melting, then their chalcophile element compositions may not have been dissimilar and the volcanic rocks *may* be used as initial estimates of the parental magma compositions. In the absence of any clearly unaltered margins to the ultramafic bodies, the initial chalcophile element contents of the magmas were therefore estimated from some of the least altered metapicrites of the Bah Lake Formation.

The measured compositions of four metakomatiitic basalts from two drill holes in the area between Pipe Pit and Ospwagan Lake are shown in **Table 9.5** and plotted on a mantle-normalized diagram in **Figure 9.46**. The samples contain between 19.9 and 23.5 wt% MgO, lie on the trend expected for phenocryst-poor, chromite-undersaturated rocks, and have Fe/Mg ratios that would be in equilibrium with the most forsteritic magmatic olivines (Fo<sub>91-93</sub>) analyzed in the ultramafic bodies of the northern TNB. Although all four samples have anomalous Cu and Au contents (presumably attributable remobilization during alteration or surface weathering) and exhibit ragged mantle-normalized chalcophile element patterns, the overall profiles resemble those of komatiites at Kambalda (e.g., Cowden et al., 1986) and have moderate to low mantle-normalized Pd/Ir ratios. When compared to typical komatiitic basalts from the Cape Smith Belt, the metapicrites of the Bah Lake Assemblage are significantly more Ir-rich, consistent with their more magnesian composition. To overcome some of the scatter in the data (in particular that for Cu and Au), the initial chalcophile element composition of the magmas from which the TNB formed was estimated from the average of the four samples plotted in **Figure 9.46**.

**Table 9.5** Composition of magma used in sulfide modelling.

	Cape Smith Belt	Kambalda (Lunnon Shoot)	Kambalda (Long Shoot)	Bah Lake Assemblage				Magma used in Modelling
MgO (wt%)	17.4	23.6	24.3	19.9	22.8	22.8	23.5	22.25
Cu (ppm)	67	68	70	152	27	122	10	78
Au	1.8	7.1	8.8	5.6	2.2	1.5	0.8	2.5
Pd	12.4	11.1	7.5	8.7	5.0	5.2	6.3	6.3
Pt	10.6			7.2	6.6	5.7	5.7	6.3
Rh	1.2			0.8	0.8	0.6	0.7	0.74
Co (ppm)	66.9			71	86	73	78	77
Ru	1.4			3.2	3.3	2.9	3.3	3.2
Ir	0.58	1.4	1.3	1.3	1.2	1.6	1.4	1.4
Ni (ppm)	654	798	1140	813	899	1222	1126	1015
[Pd/Ir] <sub>MN</sub>	13.0	6.4	4.8	5.3	3.5	2.7	3.6	4.2

All concentrations in ppb unless marked. Compositions of Kambalda komatiites and Cape Smith komatiitic basalts from Keays (1982) and Burnham & Lesher (unpubl. data), respectively.

### 9.7.2.2 Sulfide-silicate ratio (R-factor) and metal contribution from the country rocks

#### *Background*

The partitioning of an element  $i$  between a silicate magma and a sulfide magma during batch equilibration has been discussed by Campbell & Naldrett (1979), Naldrett (1981), and Campbell & Barnes (1984). If all of the sulfide is derived internally, for example by cooling, oxidation, felsification, or fractionation of the magma, the relationship between the final concentration of element  $i$  in the sulfide magma  $Y_i^f$  and the initial concentration of element  $i$  in the silicate magma  $X_i^0$  is (Campbell & Naldrett, 1979):

$$Y_i^f = \frac{X_i^0 D_i^{\text{Sul/Sil}} (R + 1)}{R + D_i^{\text{Sul/Sil}}} \quad \text{Eqn. 9.1}$$

where  $D_i^{\text{Sul/Sil}}$  is the sulfide-silicate partition coefficient, and  $R$  is the silicate:sulfide mass ratio. If all of the sulfide is derived externally, for example by desulfidation or assimilation of country rocks, the relationship is (Naldrett, 1981):

$$Y_i^f = \frac{X_i^0 D_i^{\text{Sul/Sil}} R}{R + D_i^{\text{Sul/Sil}}} \quad (\text{Eqn. 9.2})$$

These equations have been widely used in the literature to model variations in the compositions of sulfide ores in systems with variable  $R$  (e.g., Naldrett et al., 1979; Barnes & Picard, 1993; Leshner & Campbell, 1993; Lambert et al., 1998a; Maier et al., 1998; Ripley et al., 1999; Barnes & Maier, 1999). However, **Equation 2** is only applicable in special cases, and not all ore-forming systems meet the restrictions. In order to gain further insight into the restrictions (and limitations), it is necessary to return to first principles.

Mass conservation requires that the masses of element  $i$  distributed between the final silicate magma and the final sulfide magma must be equal to the masses of element  $i$  distributed between the initial silicate magma and initial sulfide magma:

$$AX_i^f + BY_i^f = AX_i^0 + BY_i^0 \quad (\text{Eqn. 9.3})$$

where  $A$  is the mass fraction of silicate magma and  $B$  is the mass fraction of sulfide magma.

Substituting  $Y_i^f = D_i^{\text{Sul/Sil}} X_i^f$ ,  $X_i^f = \frac{Y_i^f}{D_i^{\text{Sul/Sil}}}$ , and  $R = A/B$ , and rearranging, one obtains

(Leshner & Burnham, 1999, 2001):

$$Y_i^f = \frac{(X_i^0 R + Y_i^0) D_i^{\text{Sul/Sil}}}{R + D_i^{\text{Sul/Sil}}} \quad (\text{Eqn. 9.4})$$

If the assimilant contains no sulfide, then  $B^0 = 0$  and  $A^0 = 1$ , so **Equation 9.4** reduces to **Equation 9.1**. If the sulfide component of the assimilant contains none of element  $i$ , then  $Y_i^0 = 0$ , and **Equation 9.4** reduces to **Equation 9.2**. However, if  $Y_i^0 > 0$ , **Equation 9.4** *must* be used. These three situations, implications, and the appropriate mass-balance equations are summarized in **Table 9.6**; some general examples were presented by Lesher & Burnham (1999) and specific applications to Kambalda were presented by Lesher & Burnham (2001). As pointed out by Campbell & Naldrett (1979) and as is evident also from inspection of the examples presented by Lesher & Burnham (1999), if  $R > 10D$  and if  $Y_i^0 \ll X_i^0$ , the results from **Equations 1, 2, and 4** are not significantly different. However, if  $R < 10D$ , which is often the case (e.g., Naldrett et al., 1979, 1995; Lesher & Campbell, 1993; Barnes & Picard, 1993; Menard et al., 1996; Ripley et al., 1999) and may be particularly applicable to the ultramafic bodies of the TNB, or if  $Y_i^0 > X_i^0$ , which is sometimes the case (e.g., Tyson & Chang, 1984; Lesher & Campbell, 1993; Lee & Ripley, 1995; Menard et al., 1996; Thériault & Barnes, 1998), the results may be quite different.

**Table 9.6** Mass-conservation equations for two-component silicate-sulfide systems (Lesher & Burnham, 1999, 2001)

Process	Metal Balance	Mass-Balance Equation	Eq	Ref	Examples
1 Sulfide exsolved from magma	$Y_i^0 = X_i^0$	$Y_i^f = \frac{X_i^0 D_i \text{Sul/Sil}_{(R+1)}}{R + D_i \text{Sul/Sil}}$	9.1	1	Dumont, Mt. Keith-Betheno, and most other low-grade Type II strata-bound disseminated ores
2 Essentially barren sulfide incorporated by magma	$Y_i^0 = 0$	$Y_i^f = \frac{X_i^0 D_i \text{Sul/Sil}_R}{R + D_i \text{Sul/Sil}}$	9.2	2	Windarra, Langmuir, Thompson, and other deposits associated with sulfide-facies iron-formations
3 Metal-bearing sulfide incorporated by magma	$Y_i^0 > 0$	$Y_i^f = \frac{(X_i^0 R + Y_i^0) D_i \text{Sul/Sil}}{R + D_i \text{Sul/Sil}}$	9.4	3	Duluth, Kambalda, Raglan, Namew Lake, Lynn Lake?, Sudbury?, Voisey's Bay, and other deposits associated with metal-bearing country rocks

Eq: equations numbered in text. Ref: references to equations, 1: Campbell & Naldrett (1979), 2: Naldrett (1981), 3: Lesher & Burnham (1999, 2001).

### ***Metal Mixing Models***

In order to determine whether the range of chalcophile element contents observed in the ores of the TNB can reproduced solely by variations in either the ratio of silicate-sulfide magma or variable contributions from the wall-rocks, the compositions of sulfides were modelled using **Equation 9.4** above, the estimated parental magma composition, and the calculated metal concentrations in the sulfide component of different sulfide-bearing sediments (**Table**

9.7). The results of the modelling are shown in **Figure 9.47**, as plots of chalcophile element contents in 100% sulfide.

**Table 9.7** Parameters used in modeling the magmatic sulfide compositions

	Proposed Magma	Silicate- Facies IF	Sulfide- Facies IF	Ni-enriched Sulfide	D <sup>Sul/Sil</sup>
<b>Sulfur in whole-rock</b>					
S (wt%)		2.03	19.5	23.6	
<b>Metals in 100% sulfide</b>					
As (ppm)		(66)	33	18	
Bi (ppm)		3	4	(4)	
Se (ppm)		(46798)	16174	14169	3,300
Cu (ppm)	78	4373	461	2809	600
Au (ppb)	2.5	83.8	12.9	24.8	5000
Pd (ppb)	6.3	117.6	15.7	330.5	30,000
Pt (ppb)	6.3	43.4	5.6	11.6	30,000
Rh (ppb)	0.74	3.8	0.7	0.5	30,000
Co (ppm)	77	1076	50	892	50
Ru (ppb)	3.2	5.6	0.3	8.3	30,000
Ir (ppb)	1.4	2.9	0.1	0.2	30,000
Ni (ppm)	1015	6025	314	59492	175

Values in parenthesis are estimates. The abundances of metals in the SIIF, barren SUIF, and Ni-enriched SUIF have been recalculated to 100% sulfides assuming 38% S in sulfide. Partition coefficients taken from reviews by Leshner and Stone (1996) and Mathez (1999).

In each of the plots shown in **Figure 9.47**, the composition of the chalcophile elements are plotted as a function of Rh in 100% sulfide. Because Rh is a highly chalcophile element that a) should be relatively immobile in hydrothermal fluids, b) is relatively incompatible in most of the cumulate silicate phases in the ultramafic bodies, and c) is present at similar abundances in the magma and most of the sulfide portions of the potential crustal sulfide sources, it may be used to examine differences in behaviour that arise from variations in R-factor and/or metal-mixing. One advantage in comparing the chalcophile element compositions on element-element plots such as those shown in **Figure 9.47** is that the results do not require a separate calculation of the R factor for each sample and are therefore insensitive to any assumptions required in that calculation.

## Ir

There are two distinct trends evident in the plot of Ir vs. Rh:

- 1) Most of the Thompson, Birchtree, Pipe Pit, Halfway Lake, Bucko, and Manibridge samples and the single sample from William Lake plot along a linear trend with higher Ir/Rh ratios (0.5-2), similar to those of the komatiitic magma (~1.7).
- 2) Ni-rich “sedimentary sulfides” from the Thompson mine plot along a trend with generally lower Ir/Rh ratios (0.2-0.8), similar to those of the local barren sulfide-facies iron formations.

Because the Ir/Rh ratio of the different potential sources of crustal S are only marginally lower than those of the magma (0.2-0.8 vs. ~1.7), there is little difference between the different models of metal-mixing and the interaction of the magma with barren sulfide. However, the separate trend shown by the Ni-rich “sedimentary sulfides”, which have high Ni, Ir, and Rh contents, but low Ir/Rh ratios, suggest that they are not the result of *en mass*

mobilization of magmatic ores away from the ultramafic body. The significance of this will be discussed further below.

## **Ru**

The plot of Ru vs. Rh is very similar to that for Ir, except that there is a greater degree of scatter and the trends for the different crustal sulfide components diverge at low Rh contents (low R factors). In contrast to the trends shown in the Ir-Rh plot, the majority of the Ni-rich “sedimentary sulfides” plot along the trend expected for the interaction of the ultramafic magma with a component enriched in Ru relative to Rh ( $Ru/Rh = 10-20$  vs. 3 in the magma).

## **Co and Ni**

In the plots of Co and Ni vs. Rh, magmatic ores cluster at high base metal contents, indicating that  $R > 10D$ , which allowed both the silicate and sulfide phases to approach their maximum metal contents. The location of this cluster below the trend expected for Co may indicate that the value of  $D_{Co}^{Sul/Sil}$  used in the calculation (50) is too low relative to that used for Rh (30,000), even though this value is higher than the value of 30 determined empirically by Leshner and Campbell (1993).. Neither group shows any scatter towards low Ni or Co contents, suggesting that neither element has been lost relative to Rh during either magmatic or metamorphic processes.

In each plot, the Ni-rich “sedimentary sulfides” plot along the trends expected for the interaction of the magmas with a Ni-rich, Rh-poor crustal sulfide component, as represented by five Cr-poor, graphite-rich samples from Thompson mine (4) and Pipe Pit (1). If such a component were present as a unit prior to the emplacement of the ultramafic bodies and was locally thicker in the Thompson area, it would help answer the long-standing problem concerning the low volume of ultramafic material relative to Ni-Cu sulfide ore in this mine.

## **Pt**

Few, if any, of the massive sulfide samples plot on the trend expected for ores formed by the simple interaction of an ultramafic magma of the inferred composition and Ni-poor silicate-facies iron-formation, barren sulfide-facies iron-formation, or Ni-rich sulfide-facies iron-formation. As observed above (**Section 9.4.4**), almost all of the samples are depleted in Pt relative to Rh (and Pd), suggesting that i) a significant amount of Pt has been lost from the sulfides in almost all of the deposits since their formation or ii) the assumed  $D_{Pt}^{Sul/Sil}$  value was variable and less than that assumed in the calculations (30,000). These two possibilities will be discussed in more detail further below.

## **Pd**

Although the majority of the Pd contents of the massive sulfides plot along the trends expected for the interaction of an ultramafic magma with Ni-poor silicate-facies iron-formation, barren sulfide-facies iron-formation, or a Ni-rich sulfide-facies iron-formation, some of the samples from Thompson and most of those from the Pipe Pit or Birchtree have lower Pd contents, consistent with Pd loss since the formation of the ores.

Pd is more soluble under certain circumstances than the other platinum group elements, particularly Ir, and Pd/Ir ratios have been used to distinguish between hydrothermal and magmatic Fe-Ni-Cu-(PGE) sulfides (e.g., Keays et al., 1982). For example, magmatic Fe-Ni-Cu-(PGE) sulfides at Kambalda have Pd/Ir ratios of 9-10 (Cowden et al., 1986), whereas rare

hydrothermal Fe-Ni-Cu-(PGE) sulfides at Kambalda have Pd/Ir ratios of 650 or more (Leshner & Keays, 1984).

Pd is also apparently more soluble than Pt under many circumstances. Magmatic sulfides at Kambalda, Raglan, and Noril'sk have Pd/Pt ratios of ~1-3 (Naldrett, 1989), broadly similar to the host magmas, whereas hydrothermal sulfides at New Rambler have Pd/Pt ratios of ~18 (McCallum et al., 1976), and hydrothermal sulfides at Lac des Iles have Pd/Pt ratios of ~13 (Brügmann et al., 1989).

Hydrothermal quartz-sulfide  $\pm$  calcite veins at Kambalda contain significant amounts of Ni (7-12 wt%), Cu (0.1-16 wt%), Co (0.1-0.4 wt%), Se (20-250 ppm), and Pd (generally 300-1000 ppb, locally up to 73 ppm), but low abundances of Cr (30-330 ppm) and negligible amounts of Ir (<1.5 ppb) (Leshner & Keays, 1984). As a consequence, Ni/Cu, Ni/Co, and S/Se ratios are within the range of Kambalda magmatic ores, but Pd/Ir ratios (>400) are much higher than magmatic ores (<10).

The enrichment of Pd relative to Pt and Ir in hydrothermal ores is attributed to the greater tendency of Pd to form complexes with volatile elements such as As, Sb, Te, and S, which is consistent with the abundance of bismuthotellurides in these deposits. Such ores are also commonly localized at the intersections of faults and shear zones, indicating that rock permeability was critical in focussing the mineralizing fluids.

Although the Pd/Pt ratios of Thompson and Birchtree massive ores analyzed in this study range 24-92 (**Table 9.3**) and are more similar to hydrothermal ores than magmatic ores, they are largely attributable to the pronounced depletion of Pt relative to all other PGE. This is evident in comparing the abundance of Pd relative to Rh, which is more compatible but less mobile than Pt. Pd/Rh ratios are uniformly low, ranging 2-6 in 1C, T1, and Birchtree massive ores and 10-12 in 1D massive ores (**Table 9.3**). Thus, it does not appear that any of the TNB massive ores exhibit a typical hydrothermal signature.

### **Cu and Au**

The Cu and Au contents of the TNB ores show a combination of the trends shown by Co and Ni and that of Pt. Whereas a number of the samples plot along trends towards the Ni-rich sedimentary sulfides (**Fig. 9.47**), most of the massive sulfides are depleted in both Cu and Au relative to expected magmatic trends indicating that these elements have also been lost from the ores.

The data presented above indicate that two processes have been important in the genesis of the TNB Ni-(Cu-PGE) ores:

- 1) Interaction of an ultramafic magma with an externally-derived sulfide component that may have possessed a range of metal contents. Whereas the ores at Pipe and Birchtree appear to have interacted with a metal-poor component (as represented by either the sulfide- or silicate-facies iron formations present in the TNB), those at Thompson may have interacted with a component enriched in Ni, Co, Cu, and Pd. Further work is required to investigate the possibility that sills melts sedimentary sulfides with different metal contents.
- 2) Mobilization of Pt, Cu, and Au relative to Pd and Rh, as a result of a) variable extraction of the metals from the magma owing to variations in silicate-sulfide partition coefficients,



b) fractionation of the sulfide liquid, and/or c) mobilization in a hydrothermal fluid. These will be discussed in more detail below.

### 9.7.2.3 Fractionation of the sulfide liquid

Although volcanically-emplaced magmatic sulfides cool relatively quickly and do not undergo significant amounts of fractional crystallization (Leshner, 1989), intrusively-emplaced magmatic sulfides cool more slowly and, as a consequence, may fractionally crystallize monosulfide solid solution (*MSS*) from sulfide liquid (Hawley, 1965; Ebel and Naldrett, 1996, 1997). Because Cu, Au, and PPGE selectively partition into sulfide liquid compared to *MSS* (Fleet et al., 1993; Fleet and Pan, 1994; Li et al., 1996a,b; Ebel and Naldrett, 1996, 1997; Barnes et al., 1997), this process may fractionate those elements. Migration of Cu-PPGE-rich sulfides away from the main ore zone, either as liquids during emplacement or as a more ductile component during later tectonism, may lead to segregation of Cu-PPGE-rich and Cu-PPGE-poor zones, for example as observed at Sudbury and Noril'sk (Hawley, 1965; Naldrett et al., 1994a, b). Although such processes are more commonly observed in sulfides associated with mafic and intermediate magmas, which generally have lower Ni/Cu ratios, it is not clear whether this is related to the bulk composition of the ore or whether this is related to most mafic systems being intrusive. Thus, one of the questions that was to be addressed in this project was whether the low Cu, Au, Pd, and Pt contents of the TNB ores could be explained by sulfide-fractionation processes and, if so, whether there is potential to discover Cu-PPGE-rich zones associated with the known Ni-sulfide ores.

As discussed above, many TNB massive ores are depleted in Cu, Pt, Pd and Au relative to Rh on the hand-sample scale. These are the same elements that would be expected to be concentrated in the sulfide liquid during fractional crystallization of *MSS*, but the order of depletion ( $Pt \sim Cu > Au > Pd$ ) is the reverse of that expected from the experimentally-determined liquid/*MSS* partition coefficients ( $D_{Au}^{liq/MSS} > D_{Pd}^{liq/MSS} \sim D_{Pt}^{liq/MSS} > D_{Cu}^{liq/MSS}$ ; Fleet et al., 1993). Similarly, the depletion can also not be attributed to variations in R factor, because the order of depletion is different than that expected from the experimentally-determined sulfide/silicate partition coefficients ( $D_{Au}^{sul/sil} \sim D_{Pd}^{sul/sil} \sim D_{Pt}^{sul/sil} \gg D_{Cu}^{sul/sil}$ ). This indicates that the observed depletions in Cu, Au, and PPGE are not likely to have been produced by magmatic processes (i.e., variations in R factor or fractional crystallization of *MSS*), but are more likely to have been produced by metamorphic processes. Whether or not the “missing” Cu, Au, and PPGE have been concentrated into discrete zones that are amenable to exploitation is not yet known, but they may provide vectors to mineralization.

In order to better constrain the degree of depletion of Cu, Au, and PPGE, four samples of mill feed kindly provided by Inco from the Birchtree and Thompson Mines (and presumably representative the average compositions of the ores being mined at that time) were analyzed for base and precious metals. With the exception of Cu and Au, which appear to be slightly depleted, their compositions plot on or close to the calculated magmatic trends (**Fig. 9.47**), indicating that although small amounts of Cu and Au have been transported outside the mining widths, most are being recovered.

### 9.7.3 Platinum Anomaly in Massive Sulfides

The abundances of Pt in the Birchtree, Thompson, and Pipe massive ores (**Figs. 9.38, 9.39, and 9.40**, respectively) are lower than expected from our magmatic models and lower relative to the other PGEs. There are several ways that Pt may have become decoupled from the other PGEs, as discussed below.

#### 9.7.3.1 Magmatic controls on the behaviour of Pt

Bezmen et al. (1998) showed that Pd and Pt may fractionate in hydrous silicate melts under strongly reducing or strongly oxidizing conditions at 1200°C (**Fig. 9.48**). The solubility of Pd decreases from ~50 ppm to <5 ppm over the range  $fO_2$   $10^{-2}$  (HM) to  $10^{-10}$  (WI), but the solubility of Pt decreases from ~75 ppm at  $fO_2$   $10^{-2}$  (HM) to ~20 ppm at  $fO_2$   $10^{-10}$  (MW) and abruptly increases to ~50 ppm at  $fO_2$   $10^{-12}$  (WI). Thus, Pt is significantly more soluble than Pd at high  $fO_2$ , Pt and Pd have similar solubilities at moderate-low  $fO_2$ , and Pt is much more soluble than Pd at very low  $fO_2$ .

Given the nearly ubiquitous occurrence of graphitic schists in the Pipe Formation of the Ospwagan Group and graphite in the ores, it is likely that the ores formed under relatively reducing conditions. It is not clear how this would affect  $D_{Pt}^{Sul/Sil}$  and  $D_{Pd}^{Sul/Sil}$ , but if reducing conditions enhanced the solubility of Pt in the silicate melt, it is possible that this may have reduced  $D_{Pt}^{Sul/Sil}$  relative to  $D_{Pd}^{Sul/Sil}$ , resulting in the observed depletion in Pt relative to Pd (and other PPGE). If this occurred, then the silicate magmas that equilibrated with the sulfides should be less depleted in Pt than Pd. No rocks with these geochemical signatures have been identified, but this may be attributable to the dynamic nature of the ore-forming system, in which the magmas that equilibrated with the sulfides were flushed through the system.

#### 9.7.3.2 Hydrothermal controls on the behaviour of Pt

Very little experimental data are available on the solubility of PGEs in high-temperature hydrothermal or metamorphic fluids (e.g., Cook et al., 1992; Wood, 1987; Wood and Mountain, 1987; Wood, 2002). As discussed by Wood (2002), most PGE probably occur in the divalent state and, if so, “soft” ions (Pearson, 1963) like  $Pd^{2+}$ ,  $Pt^{2+}$ , and probably also  $Ru^{2+}$ ,  $Rh^{2+}$ ,  $Ir^{2+}$ , and  $Os^{2+}$ , like  $Au^+$ , should form strong complexes with soft ligands like  $HS^-$ ,  $CN^-$ , and  $I^-$ , reasonably strong complexes with the borderline soft/hard  $Cl^-$  ion, but only weak complexes with hard ligands like  $F^-$ ,  $CO_3^{2-}$ ,  $SO_4^{2-}$ , and  $PO_4^{3-}$ . Given the large amount of reduced S in the Ni-Cu-(PGE) deposits in the TNB,  $HS^-$  is expected to predominate over  $Cl^-$ .

Precipitation of Pt or Pd from a hydrothermal solution containing  $Pt(HS)_2^0$  and  $Pd(HS)_2^0$  complexes could result from a reduction of the activity of  $HS^-$ , due to boiling, oxidation, dilution, or wall-rock alteration (reaction of iron in oxides or silicates with bisulfide to form iron sulfides), but not due to changes in pH except at pH > 7-8 (Wood, 2002). Importantly, because the solubility of Pt and Pd as bisulfide complexes *decreases* between 150°C and 350°C (Wood, 2002), heating during igneous emplacement or regional metamorphism is not an effective dissolution mechanism and cooling from magmatic or high-grade metamorphic temperatures to low-grade metamorphic temperatures is not an effective depositional mechanism.

Importantly, sulfides in hydrothermal quartz veins at Kambalda (**Fig. 9.49c**) and hydrothermally-mobilized sulfides at New Rambler (McCallum et al., 1976; **Fig. 9.49f**) and Rathbun Lake (Rowell and Edgar, 1986; **Fig. 9.49f**) are very strongly depleted in Ir relative to metals of similar magmatic compatibility.

Perhaps the most relevant indication of the solubility of Au and PGE in moderate-temperature S- and Cl-bearing hydrothermal fluids are studies of volcanic-associated Cu-Zn massive sulfides (Pan and Xie, 2001). Kuroko ores, which are associated with felsic volcanic rocks, are enriched in Au but strongly depleted in all PGE (**Fig. 9.49g**), whereas Besshi ores, which are associated with mafic and sedimentary rocks, are enriched in Au, Pd, and Rh, but strongly depleted in Pt, Ru, and Ir (**Fig. 9.49g**). On the other hand, the presence of Ni and Co in As-rich vein systems such as Cobalt (Ontario) indicate that those particular metals are soluble in As-rich fluids.

Importantly, because Fe and Cu are much more abundant and much more soluble than Pt, any process that dissolves, transports, and deposits Pt (or other PGE) must also dissolve, transport, and deposit Fe and Cu. Although Pt may have been locally mobilized in metamorphic-hydrothermal fluids, the absence of highly altered wall rocks or Fe- and Cu-enriched zones suggests that Pt was not mobilized in a hydrothermal *system*.

### 9.7.3.3 Mineralogical controls on the behaviour of Pt

No Pt was detected in any of the phases analyzed in the PIXE study (see **Section 9.4.7**). We had planned to do additional work using secondary ion mass spectrometry (SIMS), which has lower detection limits, but were not able to get this work done. Although this severely limits what can be said about the mineralogical controls on Pt mobility in the TNB, data in other areas provide some general constraints.

Chyi and Crocket (1976) showed that Pd and Au in Sudbury ores are concentrated in pentlandite by a factor of ~14 relative to pyrrhotite and that Pt and Ir are concentrated in chalcopyrite by a factor of ~6 relative to pyrrhotite. However, chalcopyrite-rich veins and stringers at most magmatic sulfide deposits, including Sudbury, are enriched in Cu, Au, and PPGE relative to Ni, Co, and IPGE (see discussion by Ebel and Naldrett, 1996). Ross and Keays (1979) and Keays et al. (1981) showed that Pd in Kambalda ores is concentrated in pentlandite, that Ir is evenly distributed among sulfide phases, and that chalcopyrite is an important host for Au. Heath et al. (2001) also showed that IPGE do not fractionate between sulfide phases as much as PPGE, that Pd is concentrated in pentlandite and chalcopyrite, that Au is concentrated in pyrite, and that Ru, Rh, and Pt are concentrated in PGMs. Luguet et al. (2000) showed that pentlandites in abyssal peridotites are depleted in Pt and Au relative to Pd, Rh, Ru, Ir, and Os, but were not able to identify any Pt-rich phases, suggesting that they occurred at the sub-micron scale. Some of the apparently conflicting results of these studies may be attributable to differences in bulk composition, some to limitations in analytical methods, and some to differences in the way that the data have been presented. What is needed is complete analytical information for all of the PGE-bearing phases that can be compared with the whole-rock data to provide a mass balance. Nevertheless, within the context of the Pt depletion in the TNB, it seems clear that that Ni, Co, and IPGE do not fractionate between sulfide phases as much as Cu, Au, and PPGE, and that Pt is most likely concentrated in discrete PGMs.

If Pt was originally concentrated in PGMs, then its accessibility to metamorphic fluids would have depended on the solubilities of those phases. Additional work, involving detailed mineralogical comparisons of samples exhibiting different degrees of Pt depletion will be required to identify those phases and to confirm that hydrothermal-metamorphic processes were involved. If Pt was removed during metamorphism, then it is possible that it may have produced a halo in the surrounding rocks, which could be a valuable exploration vector.

#### 9.7.3.4 Modification of Massive Ores

Massive ores have anomalously low Cu, Au, and Pt contents relative to their Pd, Rh, Ru, Ni, and Ir contents and to the Cu and Au contents of disseminated and net-textured ores (**Fig. 9.49**). The greater solubility of these elements in hydrothermal fluids (**Section 9.7.3.2**) and the greater ductility of chalcopyrite compared to Fe-Ni sulfides (Barrett et al., 1977; McQueen, 1981a,b; McQueen, 1987) suggests that their magmatic abundances have been modified during deformation and/or metamorphism.

Massive and semi-massive “sedimentary” ores (M\$-SED and SM\$-SED) and massive ultramafic breccia ores (M\$-UB) have significantly lower Se and Cr contents and higher S/Se ratios than net-textured or disseminated ores (N\$-U or D\$-U) (**Fig. 9.49**). As sedimentary sulfides normally have significantly higher S/Se ratios (Stanton, 1972) and lower Cr contents than magmatic sulfides, this is consistent with these ores containing a much larger component of sedimentary sulfide (Eckstrand et al., 1989; Bleeker, 1990), not with secondary mobility of Se (cf. Liwanag, 2001)

Massive ores in the Thompson 1D ore body have highly variable S/Se ratios (**Fig. 9.35**). The correlations between S/Se and  $\delta^{34}\text{S}$  in the TNB and elsewhere (e.g., Groves et al., 1979; Eckstrand et al., 1989; Bleeker, 1990; Huston et al., 1995; Alirezai and Cameron, 2001) suggest that S and Se do not normally decouple during metamorphism, although they may fractionate in high T hydrothermal systems (Auclair et al., 1987; Fouquet et al., 1988). The correlations between high Se and high Ni in pyrrhotites and, to a lesser degree, pentlandites in 1D ores (**Figs. 9.29 and 9.30**) suggest a relationship between Se and Ni enrichment on both the whole-rock and mineral scale, but it is not clear whether this was a magmatic or metamorphic process (cf. Liwanag, 2001). Detailed mineral and whole-rock mass balances for individual samples involving Se, Ni, and other more and less mobile elements will be required to address this question.

1D ores have higher Pd/Ir ratios (14-22) compared to other areas in the mine (~2 to 4), but unlike hydrothermal Fe-Ni-Cu sulfides, which typically have Pd/Ir >>20 (Keays et al., 1982; Leshner & Keays, 1984), these appear to contain normal amounts of Ir and are therefore modified magmatic ores with added Pd. The correlation between high Pd and high As and Bi, together with the presence of paragenetically late (or recrystallized) Pd-bearing bismuthotellurides, gersdorffite, niccolite, and As-enriched pyrite, suggests that Pd was introduced by metamorphic fluids that traveled through the many dilatant shear zones in the mine. Bleeker (1990) noted that the As concentrations of the Thompson deposit are anomalously high (>1000 ppm As) in samples that are associated with white vein quartz deposited along a fault that runs subparallel to the ore in the Thompson 1C pit.

### 9.7.3.5 Ni Enrichment in Thompson Ores and Sediments

Pentlandites and ores in the highly deformed Thompson 1D massive sulfides have higher Ni tenors and higher Ni/Co ratios than the pentlandites in Birchtree ores and the ores in other deposits sampled in this study (**Table 9.3**). Liwanag (2001) favoured a hydrothermal-metamorphic model, in which deformation facilitated transport of Ni and Pd in As- and Bi-enriched fluids into massive ores. However, like most other deposits of this type (e.g., Western Australia: Ross and Keays, 1979; Katinni: Gillies, 1993; Namew Lake: Menard et al., 1996), there are positive correlations between Ni and *all* other chalcophile elements in TNB ores, including base metals (Cu, Co), semi-metals (As, Sb, Bi), and PGEs. The correlation between Ni and Ir (and lack of depletion of Ir relative to Ni or Co) is especially important, as hydrothermal sulfides are always strongly depleted in Ir (e.g., Keays et al., 1982; Leshner & Keays, 1984; Pan and Xie, 2001). This suggests that the Ni enrichment in the 1D ores cannot be attributed to hydrothermal-metamorphic transport and deposition.

On the other hand, the Ni-enriched metasediments analyzed by Bleeker (1990) are depleted in Pt, Ru, Ir, Os, Re, and Cr relative to normal magmatic ores (**Fig. 9.49a**). Although the data are less complete, the depletion in Ir and Cr is similar to that reported in Ni-rich metasediments at Kambalda (Paterson et al., 1984; **Fig. 9.49c**) and Langmuir (Green and Naldrett, 1981; **Fig. 9.49d**), which formed at much lower metamorphic grades (lower amphibolite and lower greenschist, respectively). Similar mineralization also occurs in the Redstone deposit (Robinson and Hutchinson, 1982), but that deposit is very strongly deformed. They differ from metamorphic-hydrothermal quartz-sulfide veins at Kambalda, which are much more strongly depleted in Ir (Leshner & Keays, 1984; **Fig. 9.49c**), and from metamorphic-hydrothermal sulfide veins in the Donaldson West deposit (Dillon-Leitch et al., 1986; **Fig. 9.49e**), which are strongly enriched in Au, Pd, Cu, and also Pt and depleted in Rh as well as Ru, Ir, and Os. Because mineralization of this type appears to occur in all localities where Type I ores are in close proximity (within ~20m) of sulfidic sediments, because it occurs in such a broad range of metamorphic environments, and because it occurs even in areas where there has been little penetrative deformation (see Paterson et al., 1984), it seems most likely that it formed via syn-magmatic *diffusion* of metals rather than being transported in hydrothermal-metamorphic fluids. If so, this suggests that Au, Pd, Cu, Rh, Ni, and Co diffuse more readily than Pt, Ru, Ir, Os, Re, and Cr, possibly because the former may occur in sulfides and diffuse more easily through sulfides, whereas the latter may occur in chromite and/or as alloys and be less easily mobilized.

Ultimately, it will be necessary to establish detailed concentration profiles in order to distinguish between mechanical mixing, fluid infiltration, and solid-state diffusion (**Fig. 9.50**).

### 9.7.4 Role of Deformation in Metal Transport

In high-strain domains, tectonized planar sulfide ore bodies are commonly localized along major shear zones and may be mobilized up to 1-2 km from their original ultramafic host (e.g., Perseverance IA shoot: Libby et al., 1998). McCallum et al. (1976) showed that sheared metagabbros at the New Rambler mine in Wyoming contained significantly greater concentrations of PGE and base metals than unsheared counterparts. They attributed this to hydrothermal leaching of PGE and base metals from gabbroic rocks and redeposition along

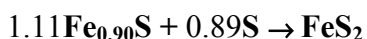
shear zones to produce Pd- and Pt-rich sulfide ores. Importantly, however, Pd and Au appear to have been mobilized relative to Pt, Rh, Ru, and Ir (**Fig. 9.49f**).

However, there is no direct evidence that metals have been transported during sulfidization processes in the TNB and, in particular, no evidence of pentlandite replacing pyrrhotite. Ni and Co appear to have only been redistributed during deformation and sulfidation: Co moved from pentlandite into pyrite and Ni moved from pyrite and pyrrhotite into pentlandite. However, it is Au, Pt, and Cu that appear to have been most mobile during deformation in the TNB and, except for Au, normally within the scale of individual ore bodies (**Figs. 9.51 and 9.52**).

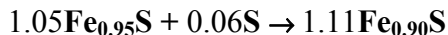
### 9.7.5 Sulfidation

The presence of hexagonal and monoclinic pyrrhotite in the ultramafic rocks and only monoclinic pyrrhotite in the massive sulfides may reflect a higher  $fS_2$  in the massive sulfides during their formation and/or addition of S to massive sulfides during deformation. Prograde metamorphism of sulfides commonly involves desulfidation (e.g., pyrite  $\rightarrow$  pyrrhotite +  $S^{2-}_{(aq)}$ ), whereas retrograde metamorphism commonly involves sulfidation (e.g., pyrrhotite +  $S^{2-}_{(aq)}$   $\rightarrow$  pyrite). Hexagonal pyrrhotite may also be converted to monoclinic pyrrhotite via oxidation (e.g.,  $4.39Fe_{0.88}S + 2O_{2(aq)} \rightarrow Fe_{0.86}S + Fe_3O_4$ ), however, this produces one mole of magnetite for each mole of monoclinic pyrrhotite and magnetite is not an abundant phase in most Thompson ores.

In diffusion experiments it is frequently observed that S diffuses much faster along fractures and in areas of high porosity than in more massive parts of the samples, which is interpreted to reflect vapour transport along grain boundaries (e.g., Condit et al., 1974). This is evident in many if not most massive ores (e.g., Barrett et al., 1977; Marston and Kay, 1980; this study), where pyrrhotite and pentlandite are commonly locally replaced by pyrite along grain boundaries via reactions of the form:



This study has also shown that disseminated ultramafic-hosted sulfides contain predominantly hexagonal (S-poor) pyrrhotite, whereas associated massive sulfides contain predominantly monoclinic (S-rich) pyrrhotite. It is possible that  $fS_2$  may have been different in disseminated and massive ores, but even in the absence of late pyrite it is possible that hexagonal pyrrhotite has been converted to monoclinic pyrrhotite via reactions of the form:



The source of the S is probably S-rich sediments in the country rocks, in which pyrite has been converted to monoclinic pyrrhotite via a reaction of the form:



Sulfide-facies iron-formations in the Pipe Formation contain primarily pyrrhotite, but rare sections examined in this study (WL95-111/223-265m) contain finely-laminated pyrite-rich zones that are replaced along the margins by porphyroblastic pyrrhotite. This indicates that significant amounts of S may have been released from the sediments in the Pipe Formation during metamorphism and would have been available to sulfidate the Fe-Ni-Cu sulfide ores.

### 9.7.6 Compositional and Mineralogical Haloes

As discussed above Ni concentrations in pyrrhotite and co-existing pentlandite grains that are disseminated within ultramafic rocks increase with increasing serpentinization (**Figs. 9.17** and **9.18**), similar to previous observations in other areas by Eckstrand (1975), Barrett et al. (1977), and Donaldson (1981). These authors attributed the changes to loss of Ni from olivine during serpentinization and uptake of Ni by the sulfide phase, combined with an increase in  $fO_2$  and  $fS_2$  during metamorphism.

This study has shown that pyrrhotite and pentlandite grains in metasedimentary sulfides in the Thompson 1C ore zone are enriched in Ni (>0.2 wt % Ni) within about 20 metres of the ultramafic body and within about 20 metres of the adjacent massive magmatic sulfide horizons. The Ni enrichment in pyrrhotite and pentlandite coincides with an increased modal abundance of pentlandite in the metasedimentary rocks. Monoclinic pyrrhotite dominates over hexagonal pyrrhotite in the massive sulfides and in metasedimentary rocks within tens of metres of the massive sulfides. Thus, the Ni halo around the massive sulfide horizons is therefore both compositional and modal.

During high-temperature metamorphism, new mineral assemblages and metamorphic textures often form around ore bodies. For example, Nesbitt and Kelly (1980) and Nesbitt (1982) showed that during peak metamorphism at Ducktown (Tennessee), the log  $fS_2$  and log  $fO_2$  within massive sulfides were  $-2.5$  and  $-18.5$ , respectively, whereas the values within the country rocks were  $-7.0$  and  $-21.4$ , respectively. These data indicate that the ore bodies were more oxidizing and more sulfidizing than the host rocks, causing O and S to move from the ores to the country rocks, sulfidating Fe-rich silicates and Fe-Ti-oxides. Importantly, however, no reactions of this type have been observed around the Thompson ore bodies, suggesting much more limited mobility of S in the TNB.

## 9.8 Conclusions

- 1) Sulfide minerals in massive ores (M\$-UB and M\$-SED) in the Thompson, Birchtree, and William Lake deposits show strong evidence of metamorphic modification on both the hand specimen and thin-section scale, indicating that the ores were emplaced prior to peak metamorphism and most of the deformation.
- 2) Although chalcopyrite appears to have been concentrated along the contacts between massive sulfide horizons and metasedimentary country rocks during metamorphism, there does not appear to have been significant loss of a fractionated Cu-liquid at the magmatic stage, owing most likely to the high Ni and low Cu contents of the original sulfide melt, suggesting that there is not much potential for Cu-rich stringer zones within the country rocks in the TNB.
- 3) The chalcophile element compositions of the ores may be successfully modelled by the interaction of an ultramafic magma and an externally derived sulfide melt with a range of initial metal contents.
- 4) Although the chalcophile element composition of the parental magma may have been similar to that of the most magnesian Bah Lake Formation metapicrites, such similarities are insufficient to prove or disprove a co-magmatic relationship between the sills and the volcanic rocks.

- 5) Although mobilization of metals during metamorphism appears to have moved Cu, Au, and Pt from massive sulfides into the adjacent country rocks, the majority of the metals appear to have remained within the current mining widths and are being recovered.
- 6) During emplacement of the magmatic massive sulfides, Ni and Co appear to have diffused up to 20m into the metasedimentary wall rocks to create Ni-enriched metasedimentary ores. Although only useful over a relatively short distance, such enrichment may provide a vector towards mineralization during exploration.

## 9.9 Further Work

- 1) Although we planned to carefully investigate the mobility of Ni during metamorphism, the samples that taken by Liwanag (2001) that were thought to be Ni-rich sediments (M\$-SED) ended up being, based on geochemical comparisons with the work of Bleeker (1990), mobilized massive sulfides (M\$-UM). We consulted Inco and Falconbridge geologists and tried to identify other areas where the transition from M\$-UM through M\$-SED to MS-SED could be sampled, but were not able to find a suitable area to sample. Any attempts to further constrain the degree and nature of Ni mobilization will require access to a very carefully-controlled sample suite.
- 2) Ni has been interpreted to partition more strongly into sulfides than olivine at metamorphic temperatures than at magmatic temperatures. This is broadly consistent with the tendency of most elements to partition less strongly (positively or negatively) at higher temperatures because of greater bond vibrations and less limitations on crystal structural controls, however, it is also possible that this is an R effect. Sulfides typically equilibrate with larger amounts of silicate magma than they do with olivine at the metamorphic stage. Thus, it is entirely possible that the temperature effect may be even larger once the R factor effect is taken into account. This would have important implications for the beneficiation of Type II disseminated sulfide mineralization.